Plakophilin 3 mediates Rap1-dependent desmosome assembly and adherens junction maturation

Viktor Todorović[a], Jennifer L. Koetsier[a], Lisa M. Godsel[a,b], and Kathleen J. Green[a,b,c]
[a]Department of Pathology, [b]Department of Dermatology, and [c]R.H. Lurie Comprehensive Cancer Center, Northwestern University Feinberg School of Medicine, Chicago, IL 60611

ABSTRACT **The pathways driving desmosome and adherens junction assembly are temporally and spatially coordinated, but how they are functionally coupled is poorly understood. Here we show that the Armadillo protein plakophilin 3 (Pkp3) mediates both desmosome assembly and E-cadherin maturation through Rap1 GTPase, thus functioning in a manner distinct from the closely related plakophilin 2 (Pkp2). Whereas Pkp2 and Pkp3 share the ability to mediate the initial phase of desmoplakin (DP) accumulation at sites of cell–cell contact, they play distinct roles in later steps: Pkp3 is required for assembly of a cytoplasmic population of DP-enriched junction precursors, whereas Pkp2 is required for transfer of the precursors to the membrane. Moreover, Pkp3 forms a complex with Rap1 GTPase, promoting its activation and facilitating desmosome assembly. We show further that Pkp3 deficiency causes disruption of an E-cadherin/Rap1 complex required for adherens junction sealing. These findings reveal Pkp3 as a coordinator of desmosome and adherens junction assembly and maturation through its functional association with Rap1.**

Monitoring Editor
Asma Nusrat
Emory University

Received: May 12, 2014
Revised: Aug 26, 2014
Accepted: Sep 4, 2014

INTRODUCTION

Desmosomes are cell–cell junctions that tether the intermediate filament (IF) cytoskeleton to plasma membrane–spanning desmosomal cadherins through a complex comprising Armadillo (Arm) proteins (plakoglobin [Pg] and plakophilins 1–3 [Pkps 1–3]) and the IF-associated protein desmoplakin (DP; Holthofer *et al.*, 2007; Delva *et al.*, 2009). Loss of tissue integrity due to failure of desmosomal adhesive function is considered a major underlying cause of inherited, autoimmune, and bacterial toxin–mediated disorders of skin and heart (Amagai and Stanley, 2012; Campuzano *et al.*, 2013; Kitajima, 2013). However, far from being inert spot welds holding cells together, desmosomes are dynamic structures whose assembly state is sensitive to alterations in signaling that occur during differentiation, wound healing, and disease pathogenesis (Green *et al.*, 2010; Kowalczyk and Green, 2013). Although classic cadherin-associated Arm proteins such as β-catenin and p120 catenin have well-established functions that transcend adhesion, we know less about extrajunctional roles of the desmosomal Arm proteins.

Recently Pkps have emerged as Arm proteins that function not only in adhesion, but also in recruiting signaling molecules to desmosomes and their precursors necessary for regulating desmosomal dynamics (Bass-Zubek *et al.*, 2009). Plakophilins are members of the Arm family of proteins most closely related to p120 catenin (Bass-Zubek *et al.*, 2009). Each of the Pkps 1–3 has a specific pattern of tissue expression (Heid *et al.*, 1994; Mertens *et al.*, 1996; Moll *et al.*, 1997; Schmidt *et al.*, 1999; Goossens *et al.*, 2007; Pieperhoff *et al.*, 2008), multiple splice variants that localize to distinct cellular compartments (Mertens *et al.*, 1996; Schmidt *et al.*, 1997), and multiple specific binding partners (Hofmann *et al.*, 2000; Chen *et al.*, 2002; Bonne *et al.*, 2003). Although some redundancy exists in their core role of ensuring tissue integrity (Sklyarova *et al.*, 2008), published data suggest that Pkp family members also mediate specific adhesion-dependent and -independent functions (Hatzfeld *et al.*, 2000; Sobolik-Delmaire *et al.*, 2010; Wolf *et al.*, 2010, 2013; Kirchner *et al.*, 2012; Moriarty *et al.*, 2012; Munoz *et al.*, 2012; Koetsier *et al.*, 2013). Pkp3 was the last of the plakophilin family members to be discovered (Schmidt *et al.*, 1999). Although it is down-regulated in various

This article was published online ahead of print in MBoC in Press (http://www.molbiolcell.org/cgi/doi/10.1091/mbc.E14-05-0968) on September 10, 2014.
Address correspondence to: Kathleen J. Green (kgreen@northwestern.edu).
Abbreviations used: Arm, Armadillo; DP, desmoplakin; Dsc2, desmocollin 2; Dsg, desmoglein; E-cad, E-cadherin; FSK, forskolin; IF, intermediate filament; ISO, isoprenaline; Pg, plakoglobin; PKA, protein kinase A; PKC, protein kinase C; Pkp, plakophilin; PROP, propranolol; PV, pemphigus vulgaris.

cancers (Furukawa *et al.*, 2005; Aigner *et al.*, 2007; Valladares-Ayerbes *et al.*, 2008, 2010; Takahashi *et al.*, 2012) and has been shown to interact with RNA-binding proteins and stimulate eIF4A1-dependent translation (Hofmann *et al.*, 2006; Wolf *et al.*, 2010), there is very little knowledge about Pkp3's functions and functional interactions at the cellular and molecular levels (Hofmann *et al.*, 2006; Wolf *et al.*, 2010).

In response to de novo cell–cell contact or elevation in extracellular calcium concentration, classic and desmosomal cadherin-based junction assembly is initiated in epithelial cells (Penn *et al.*, 1987; Pasdar and Nelson, 1989; Adams *et al.*, 1998; Green *et al.*, 2010). The formation of actin-associated adherens junctions and IF-associated desmosomes are tightly coupled events. Although the molecular mechanisms responsible for integrating the two processes are poorly understood, remodeling of the actin cytoskeleton that occurs in response to upstream ligation of classic cadherins is important for assembly of the desmosomal plaque. In contrast to the rapid, microtubule-dependent transport of cadherin-containing vesicles (Nekrasova *et al.*, 2011), the obligate desmosomal plaque component DP reaches sites of junction assembly in three phases. In response to cell–cell contact, Pkp2 and, shortly thereafter, DP rapidly accumulate at the membrane in phase 1, followed by formation of nonvesicular cytoplasmic Pkp2/DP-containing desmosome precursors in phase 2 (20–30 min from contact). In phase 3, these non–membrane bound precursors move toward and merge with the nascent cell–cell contacts in an actin- and myosin-dependent manner (Godsel *et al.*, 2005, 2010). Our lab recently demonstrated that Pkp2 not only needs to bind to DP, but also needs to harness signaling activities of molecules such as protein kinase C α (PKCα) and RhoA in order to facilitate their accumulation at sites of junction assembly and usher DP from cytoplasmic particles to nascent desmosomes (Bass-Zubek *et al.*, 2008; Godsel *et al.*, 2010). However, the functional interactions between DP and other desmosomal molecules needed for its loading into the cytoplasmic particles, transport to membrane, and incorporation into desmosomes are not yet known. Similarly, our understanding of the molecular machinery and associated signals that couple the adherens junction and desmosome assembly cascades is incomplete.

Here we show that Pkp3 plays essential roles in desmosome formation that are largely distinct from those of related Pkp2. We establish that Pkp3, through its functional interaction with Rap1, coordinates the assembly states of two major cadherin-based junctions—desmosomes and adherens junctions. Our data suggest that whereas either Pkp2 or 3 is able to initiate phase 1 recruitment of DP to the sites of nascent cell–cell contacts, Pkp3 mediates the assembly of cytoplasmic desmosome precursors (phase 2), which are then transported to the membrane in a Pkp2-dependent manner (phase 3). Pkp3-deficient cells fail to properly assemble desmosomes and exhibit weakened intercellular adhesion. Second, we characterize Pkp3 as a novel Rap1 GTPase binding partner, harnessing its activity to promote desmosome assembly and cell–cell adhesion integrity. Finally, we show that Pkp3 ablation leads to disruption of the E-cadherin (E-cad)/Rap1 complex concomitant with the failure of E-cad to form properly sealed adherens junctions. Taken together, our data support the idea that Pkp3 coordinates desmosomal and adherens junction assembly and maturation through functional interactions with Rap1.

RESULTS

Pkp3 is required for desmosome integrity

To determine the role of Pkp3 in desmosome structure and function, we introduced Pkp3 and, for comparison, Pkp2 small interfering RNA (siRNA) pools (for analysis of individual sequences of the Pkp3 pool, see Supplemental Figure S1, A, B, and D–F) into SCC9 cells. This resulted in nearly total loss of respective targets without affecting the steady-state expression of other desmosome components, including compensatory expression of other plakophilins (Figure 1A). In Pkp3 knockdown (KD), localization of other desmosome components at cell–cell interfaces was aberrant. Desmoglein 2 (Dsg2), desmocollin 2 (Dsc2), and Pkp2 all exhibited a more discontinuous punctate distribution at cell–cell interfaces, as observed by immunofluorescence analysis of confluent monolayers (Figure 1B). In addition, Pg showed similar, albeit less pronounced disruption (Figure 1B). Similarly, ultrastructural comparison of Pkp3 KD cells with control cells revealed the presence of tightly clustered desmosomes (Figure 1C) separated by long stretches of membrane with no desmosomes. Moreover, Pkp3 KD cells exhibited significant variability in desmosome length and width compared with control cells, with some very large desmosomes present (Figure 1, C and D). Changes in desmosome morphology and a reduction in desmosome number correlate with weaker cell–cell adhesion (McMillan and Shimizu, 2001), so we next tested whether the strength of cell–cell adhesion was affected in Pkp2- and Pkp3-deficient cells. Cell monolayers lifted as a single sheet by using the enzyme dispase were subjected to sheer stress. Ablation of either protein increased the cell sheet fragmentation by approximately eightfold, with double knockdown resulting in complete loss of monolayer integrity (Figure 1E).

Pkp3 is required for desmosome assembly

Because DP is an obligate desmosome component that serves as a general marker of junction assembly state, we next tested how ablating Pkp3 affects its cellular localization. In steady state, most DP is localized at cell–cell contacts (Figure 2A and Supplemental Figure S1, B, C, E, and F). Frequently, some unincorporated cytoplasmic particles can be observed in the cortical region adjacent to the plasma membrane, but these are fewer than what can be observed during de novo assembly of desmosomes. Pkp2 KD cells exhibit the previously reported "beads-on-a-string" appearance characterized by the alignment of cytoplasmic DP particles along intermediate filaments and reduced DP at cell–cell contacts (Bass-Zubek *et al.*, 2008; Figure 2A, see lower high-magnification inset). In contrast to the "beads-on-a-string" appearance of Pkp2-ablated cells, Pkp3 KD SCC9 and HaCaT cells exhibited a diffuse cytoplasmic DP localization with large DP clusters at the sites of cell contact, albeit sparsely distributed along the border (Figure 2A and Supplemental Figure S1, C and E). Pkp2/3 double-KD cells exhibited only diffuse DP cytoplasmic staining, with no DP present at the cell borders (Figure 2A). The restricted distribution of DP along the plasma membrane in Pkp3 KD cells correlated with a significant decrease in average fluorescent intensity of DP at cell–cell interfaces. A concomitant increase in cytoplasmic intensity of DP was observed in Pkp3-silenced cells compared with control cells (Figure 2B). This effect of Pkp3 ablation on DP redistribution from the cell–cell borders to a more diffuse cytoplasmic distribution is preserved in a three-dimensional (3D) organotypic model that recapitulates the differentiation and morphogenesis program exhibited by developing epidermis (Figure 2, C and D). In contrast to Pkp3-null mice (Sklyarova *et al.*, 2008), Pkp3-silenced human raft cultures do not exhibit compensatory overexpression of Pkp1, and the presence of Pkp1 (Supplemental Figure S1G) does not seem to be able to compensate for Pkp3 loss in providing for proper DP localization at the sites of cell–cell contact.

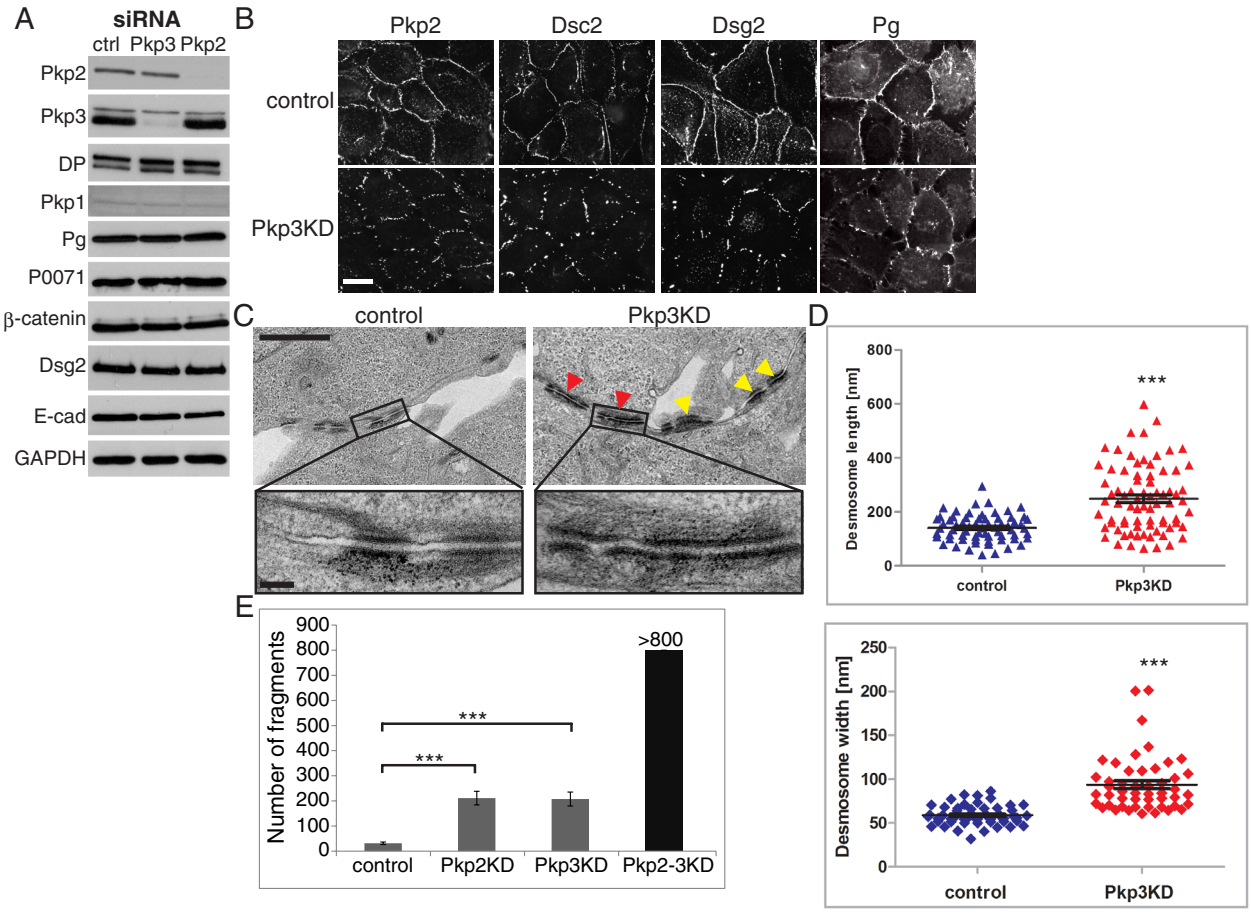

FIGURE 1: Pkp3 ablation disrupts desmosomes. (A) Western blot showing no change in the levels of indicated desmosomal and adherens junction molecules in SCC9 cells in Pkp2 and 3 siRNA knockdown. (B) Immunofluorescence showing punctate Pkp2, Dsc2, Dsg2, and Pg staining at the sites of cell–cell contacts in Pkp3 KD SCC9 cells compared with control. Scale bar, 20 μm. (C) Electron micrographs demonstrating changes in size (yellow arrows, large, single desmosomes) and morphology (red arrows, large, tandem desmosomes) of desmosomes in Pkp3 KD as compared with the control SCC9 cells. Scale bar, 1 μm, 100 nm (enlargements). (D) Scatter plots showing an increase in length (top; triangles) and width (bottom; diamonds) of individual desmosomes observed by electron microscopy in control (blue) and Pkp3 KD (red). Horizontal lines represent mean ± SEM. ***$p < 0.001$ (*t* test). (E) Bar graph representing weakening of cell–cell adhesion (measured as cell monolayer fragmentation) for Pkp2, 3, and double KD. Error bars are ± SEM. ***$p < 0.001$ (ANOVA, Bonferroni). Note: Pkp2-3 double KD caused excessive fragmentation, so only up to 800 fragments were counted.

Pkp3 deficiency prevents DP recruitment to desmosome precursor particles

The presence of diffuse cytoplasmic DP staining in Pkp3-silenced cells raises the possibility that Pkp3 may regulate DP incorporation into cytoplasmic desmosome precursors that are subsequently transported to the sites of cell–cell contact. To test this hypothesis, we subjected cells to fractionation and then analyzed the DP content in saponin-soluble cytosolic and saponin-insoluble fractions. In steady-state conditions there is a clear shift of DP from the keratin 18 (intermediate filament cytoskeleton component)–containing, saponin-insoluble fraction into the cytosol (Figure 3A). Moreover, this shift failed to occur in the Pkp2-ablated cells. To discern whether DP fractionation was affected during desmosome assembly, we incubated SCC9 cells in low-calcium medium to allow for existing desmosomes to disassemble and then switched them back to high calcium (calcium switch) to monitor desmosome assembly over time. Upon calcium switch, a steady decrease of DP in the saponin-soluble cytosolic fraction was observed in the control cells over time following the switch. In contrast, in Pkp3-ablated cells, DP remained primarily in the saponin-soluble fraction throughout the time course (Figure 3B). These results suggest that whereas most of the cytoplasmic DP in control cells is recruited into desmosomes and desmosome precursors, in Pkp3-silenced cells most of it remains in cytosol. We next visualized DP distribution in the cells by immunofluorescence. Whereas in the control cells the amount of DP at the borders steadily increases at the expense of cytoplasmic DP after calcium-induced desmosome assembly initiation, DP failed to be cleared from the cytoplasm in Pkp3 KD cells (Figure 3, C and D). The analysis of the size of the DP particles at cell–cell borders in steady-state conditions reveals an increase (Figure 3E), indicating possible aberrant coalescence in the Pkp3 KD cells (see later discussion).

Pkp3 deficiency leads to aberrant coalescence of the DP particles at the plasma membrane

To enhance the temporal resolution of DP trafficking to sites of newly forming cell–cell contacts, we next performed live-cell imaging on well-characterized doxycycline-inducible, green fluorescent protein (GFP)–tagged DP-expressing A431 cells (Godsel *et al.*, 2005)

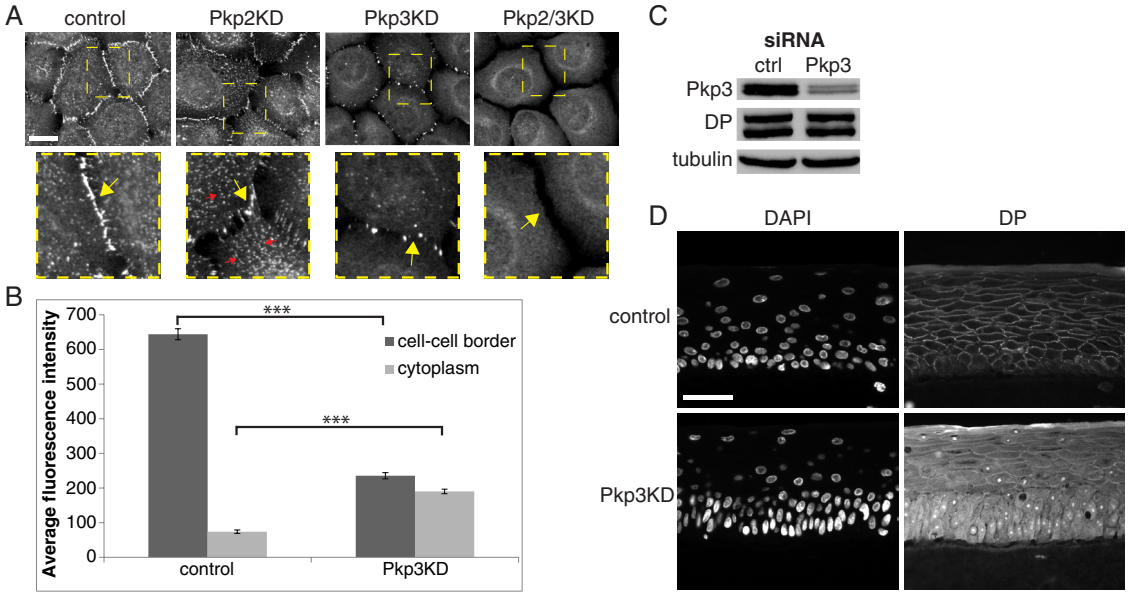

FIGURE 2: Pkp3 is required for efficient assembly of DP into desmosomes. (A) Immunofluorescence staining for DP representing the distinct patterns of its disruption in Pkp2, Pkp3, and Pkp2-3 double-KD SCC9 cells. Scale bar, 20 μm. Yellow dashed rectangles in top images delineate areas enlarged at the bottom. Yellow arrows point to the sites of cell–cell contacts; red arrows point to DP-containing nonvesicular desmosome precursors in the cytoplasm. Note the absence of cytoplasmic particles in Pkp3 KD and both particles and cell–cell border DP in double-KD cells. (B) Average fluorescence DP pixel intensity at the cell–cell borders and inside the cytoplasm, measured for ≥100 individual cells, showed decreased DP at cell–cell borders in Pkp3 KD cells and a corresponding increase in the cytoplasm. Error bars represent ± SEM. ***$p < 0.001$ (ANOVA, Bonferroni). (C) Western blot showing the efficiency of Pkp3 siRNA KD in 3D organotypic raft after 6 d of culture. (D) Representative immunofluorescence images of 3D raft cultures after 6 d of differentiation show diffuse cytoplasmic DP distribution in Pkp3-ablated rafts. Scale bar, 50 μm.

coming into contact after scratch wounding (Figure 4 and Supplemental Videos S1 and S2). In control cells, the relative fluorescence intensity of DP increased both during initial phase 1 coalescence at the membrane and as precursors incorporated into the maturing border during phase 3 (Figure 4, A and B). In Pkp3 KD, the initial phase occurs, but the corresponding increase in DP accumulation during junction maturation appeared to be abolished (Figure 4A), resulting in a plateauing of the DP fluorescence intensity after phase 1 (Figure 4B). However, this leveling off belies the striking difference in DP particle dynamics at the borders of Pkp3 KD cells compared with control. Phase 3, during which particles assembled in the cytoplasm in phase 2 translocate and incorporate into the cell–cell border (Godsel *et al.*, 2005), starts ~40 min upon initial cell–cell contact. In contrast, in Pkp3 KD cells, this phase is missing. Instead of steady growth in both the numbers and fluorescence intensity of junctional DP particles observed in the control, Pkp3 KD cells exhibit extensive lateral DP particle coalescence and concomitant decrease in number (Figure 4, A–C, and Supplemental Video S2). Large structures formed in this manner may correspond to the clustered desmosomes observed by electron microscopy (Figure 1C).

Adenylyl cyclase activation rescues the effects of Pkp3 deficiency on desmosome assembly and cell–cell adhesion

We previously showed that PKCα activation and inhibition of sustained RhoA activity restored proper desmosome assembly and allowed for DP border localization in Pkp2-ablated cells (Bass-Zubek *et al.*, 2008; Godsel *et al.*, 2010). To test whether any of the aforementioned pathways are involved in Pkp3-dependent desmosome assembly, we treated control and Pkp2 and 3 KD keratinocytes with a PKC activator (phorbol 12-myristate 13-acetate [PMA]), a RhoA inhibitor (C3), and an adenylyl cyclase activator (forskolin [FSK]). Activation of PKC and RhoA inhibition restored normal DP localization in Pkp2 KD cells, as expected (Figure 5A). In contrast, DP cell–cell border localization was not rescued by these treatments in Pkp3 KD cells (Figure 5A and Supplemental Figure S2A). However, activation of cAMP production by FSK treatment (Supplemental Figure S2B) restored DP localization upon Pkp3 KD but had no effect on Pkp2 KD, illustrating that Pkp3 and Pkp2 modulate DP localization/trafficking via different pathways (Figure 5A). Two-day FSK treatment of organotypic epidermal cultures differentiated over a 6 d period also restored DP to its proper location in Pkp3 KD rafts (Figure 5B), demonstrating that adenylyl cyclase activation can still rescue the effects of Pkp3 ablation in differentiating keratinocytes and in the presence of Pkp1. To test whether inhibition of cAMP production could recapitulate the DP phenotype observed in Pkp3-silenced cells, we treated cells with the β-adrenergic receptor antagonist propranolol (PROP) and its agonist isoprenaline (ISO) as a control. As expected, treatment with ISO restored DP border localization in Pkp3 KD cells similarly to FSK, whereas treatment with PROP caused a disruption of DP border localization (Figure 5, C–E). At the same time, treatment of Pkp3 KD cells with either FSK or ISO completely restored cell–cell adhesion strength to detached monolayers, whereas treatment with PROP disrupted cell–cell adhesion to the level similar to that observed in Pkp3 KD (Figure 5F).

Pkp3-dependent activation of Rap1 is required for desmosome assembly in keratinocytes

The secondary messenger cAMP is responsible for regulating two major signaling axes: protein kinase A (PKA) activation and activation of the Rap1 pathway through the guanine exchange factor

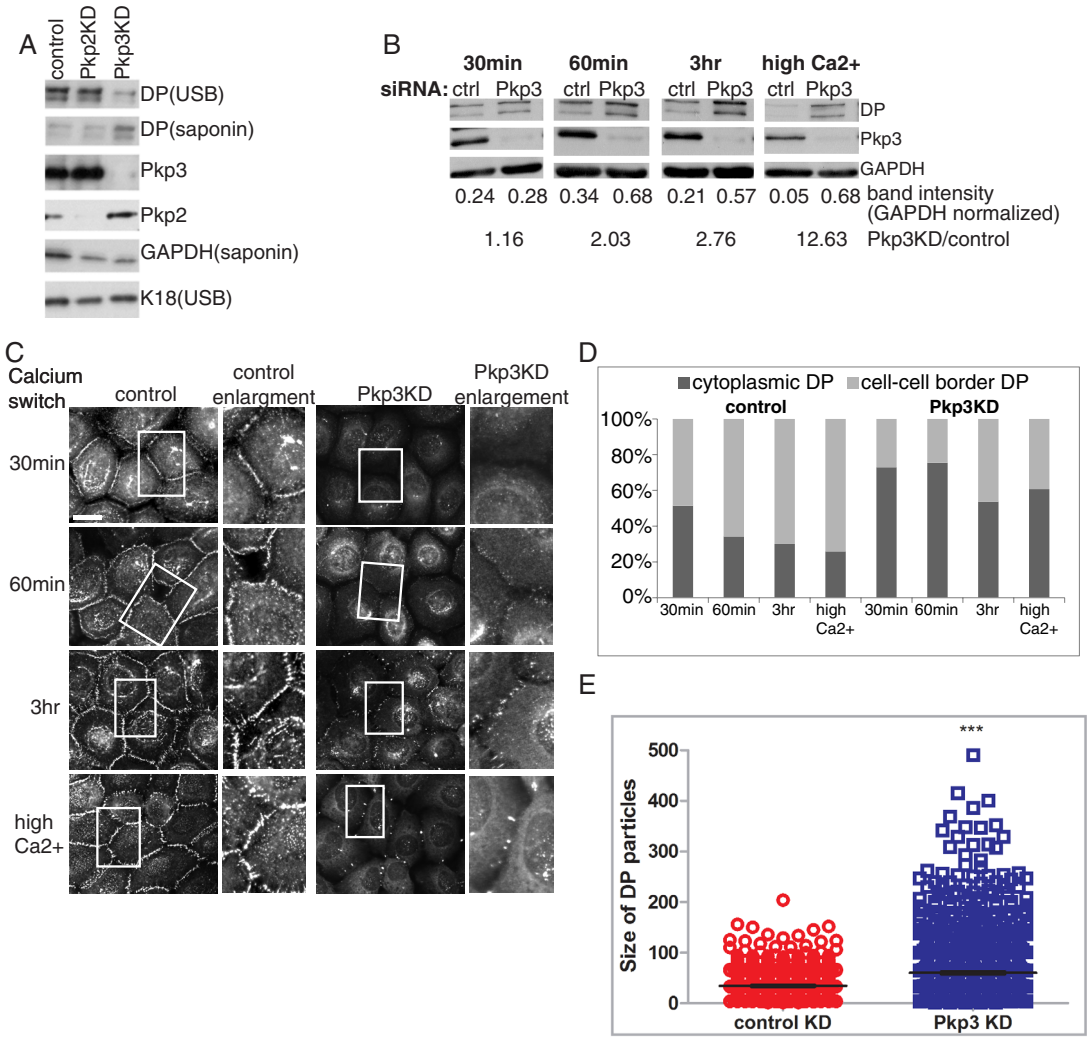

FIGURE 3: Pkp3 mediates recruitment of soluble cytoplasmic DP to the sites of cell–cell contacts. (A) Western blot showing the difference in the presence of DP in cytoplasmic (saponin soluble) and membrane/cytoskeleton-bound (urea soluble) fractions in Pkp3 KD cells compared with control and Pkp2 KD cells. GAPDH and keratin 18 (K18) were used as loading controls for their respective fractions. (B) Western blot showing the levels of DP in the cytoplasmic (saponin soluble) cell fraction under conditions of calcium switch. GAPDH- normalized DP band intensity for each condition was determined using ImageJ. Ratio between soluble cytoplasmic DP in control and Pkp3 KD cells shows a rapid decrease in cytoplasmic DP in control cells. (C) Representative immunofluorescence images of DP appearing at cell borders after calcium switch from low to calcium concentration permissive for cell–cell junction formation, after the time indicated. "High Ca2+" represents cells that were switched overnight and are identical to steady-state conditions. White solid rectangles in the images to the left delineate areas enlarged at the right. Scale bar, 20 μm. (D) Ratio between the average fluorescence pixel intensities of cell–cell border and cytoplasmic DP and average total DP fluorescence intensity in the conditions depicted in C shows that shift of DP from cytoplasm to cell–cell border is largely absent in Pkp3 KD cells. Average total fluorescence intensity was normalized to represent 100% in each condition. The *p* values for control-to-Pkp3 KD comparisons are as follows (ANOVA, Bonferroni): 30 min cytoplasmic DP: ns, $p > 0.05$. All other cytoplasmic and cell–cell border DP measurements: $p < 0.001$. (E) Scatter plot quantifying the increase in DP particle size at the cell–cell borders of Pkp3KD cells compared to controls, as shown in part C, high Ca2+ condition. Horizontal lines represent mean ± SEM. ***$p < 0.001$ (*t* test). Number of individual particles analyzed is 1066 for control and 1148 for Pkp3 KD.

(GEF) exchange protein directly activated by cAMP (EPAC; Kopperud *et al.*, 2003; Cheng *et al.*, 2008). Despite our early findings that FSK treatment leads to DP phosphorylation and enhances its accumulation at cell–cell interfaces (Stappenbeck *et al.*, 1994; Godsel *et al.*, 2005), the PKA inhibitor H89 fails to disrupt DP border localization in keratinocytes (Bass-Zubek *et al.*, 2008; Supplemental Figure 3C). In addition, phosphorylation of CREB, a major downstream target of PKA, is not significantly changed upon Pkp3 ablation in SCC9 and A431 cells (Supplemental Figure S3, A and B). These observations suggest that the cAMP/PKA pathway does not contribute directly to desmosome assembly. Because the only other major cAMP target is EPAC, we tested whether its activator, 8-CPT-2Me-cAMP restores, DP at the sites of cell–cell contacts in Pkp3-deficient cells. As shown in Figure 6, A and B, EPAC stimulation rescued DP accumulation at cell–cell borders in Pkp3- silenced cells. Therefore we proceeded to determine whether the EPAC downstream effector Rap1 GTPase is

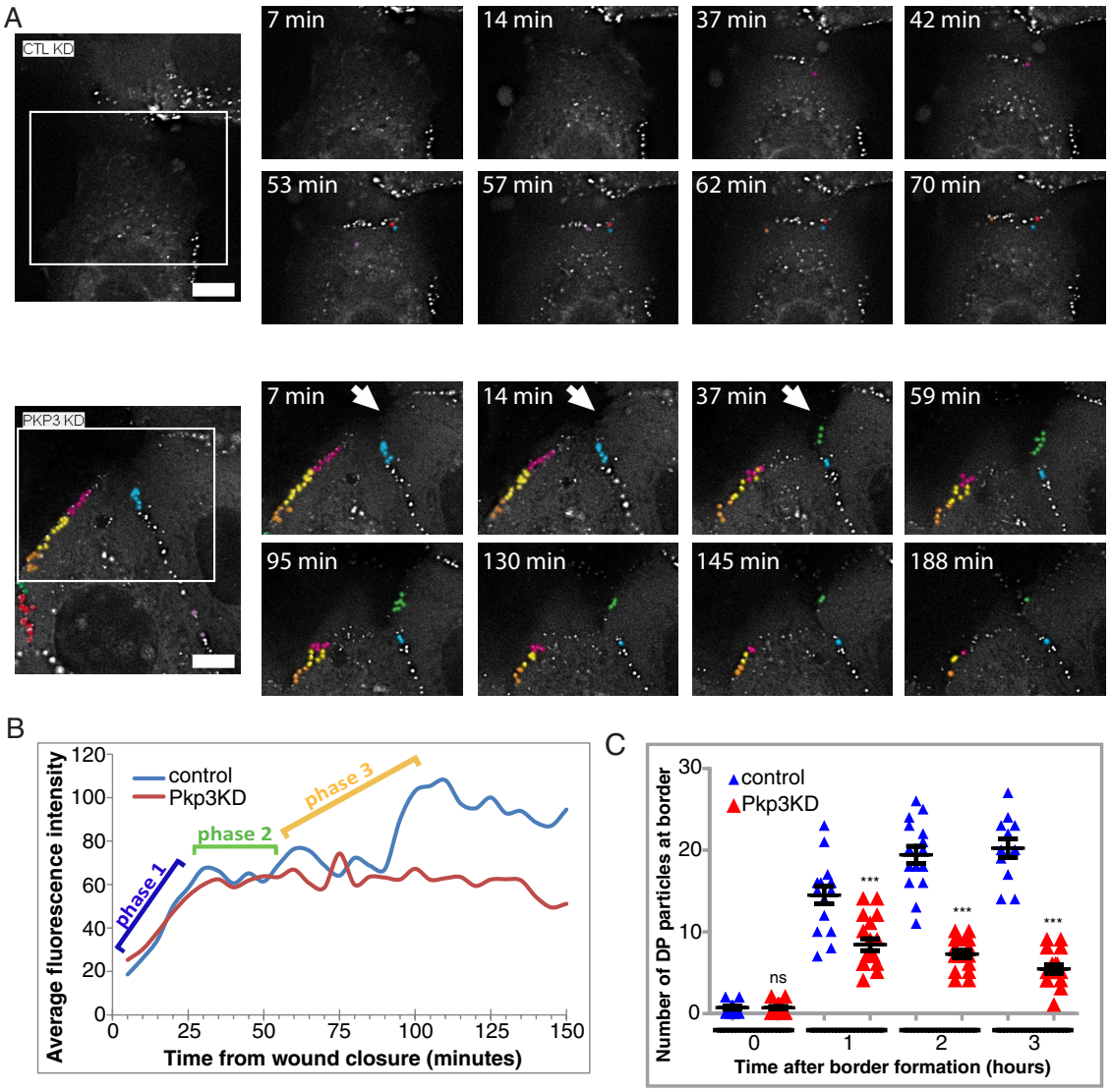

FIGURE 4: Pkp3 deficiency leads to aberrant coalescence of DP at cell–cell borders. (A) Representative still images taken from the Supplemental Videos S1 and S2 showing appearance of DP at the borders at times indicated. In control cells, indicated times coincide with the wound closure. In Pkp3KD cells, white arrow indicates the closing wound starting at 14 min. White solid rectangles to the left delineate regions enlarged at the right. DP cytoplasmic and membrane particles in control and Pkp3 KD cells, respectively, were colorized as follows: pink, purple, orange, red, and blue to highlight cytoplasmic DP precursors migrating into the cell–cell border in control cells; red, dark green, orange, yellow, pink, blue, and purple to highlight membrane DP coalescing at the sites of cell–cell contacts in Pkp3KD cells; and green to highlight DP appearing, then coalescing, at the site of newly forming cell–cell border in Pkp3KD cells. Scale bar, 20 μm. (B) Graph representing average fluorescent pixel intensities of DP present at the sites of representative cell–cell contacts, measured every 5 min in A431 cells establishing new cell–cell junctions upon wound closure. Blue, green, and orange brackets indicate phases 1–3 in control cells, respectively. (C) Vertical scatter plot representing the number of DP particles present at individual borders at times indicated during live-cell imaging experiments. Number of borders analyzed: control, 16; Pkp3 KD, 18. Fewer borders were analyzed for 3-h time point, as not all border formation was followed by live-cell imaging for 3 h: control, $N = 12$; Pkp3 for KD, $N = 17$. Bars represent mean ± SEM. ns, $p > 0.5$, ***$p < 0.0001$ (ANOVA, Bonferroni).

involved in Pkp3-mediated desmosome assembly. To discern whether Pkp3 KD affected Rap1 activity, we performed pull-down assays for GTP-bound Rap1 in normal human keratinocytes after a calcium switch. Consistent with previous data showing that Rap1 activity is elevated in keratinocytes switched to high calcium (D'Silva *et al.*, 2003), in control cells, Rap1 activity increased 5 and 60 min after the calcium switch, whereas no such increase was observed in Pkp3 KD cells (Figure 6C). Finally, overexpression of wtRap1-GFP (Figure 6D) efficiently rescued DP border localization in Pkp3 KD cells (Figure 6, E and F).

Pkp3/Rap1 complex is required for Rap1/E-cad interaction

To address whether Pkp3 governs Rap1 activity through a physical association, we first gauged whether the two proteins exist in close proximity in situ, using a proximity ligation assay (PLA). Our results indicate that Pkp2 and Pkp3 are both found in close association with DP, as predicted, whereas only Pkp3 is found to be in close proximity with Rap1 (Figure 7A). To test biochemically whether Pkp3 interacts with Rap1, we performed immunoprecipitation experiments. The data show Pkp3 being specifically precipitated with anti-Rap1 antibody, whereas this is not the case with Pkp2 (Figure 7B).

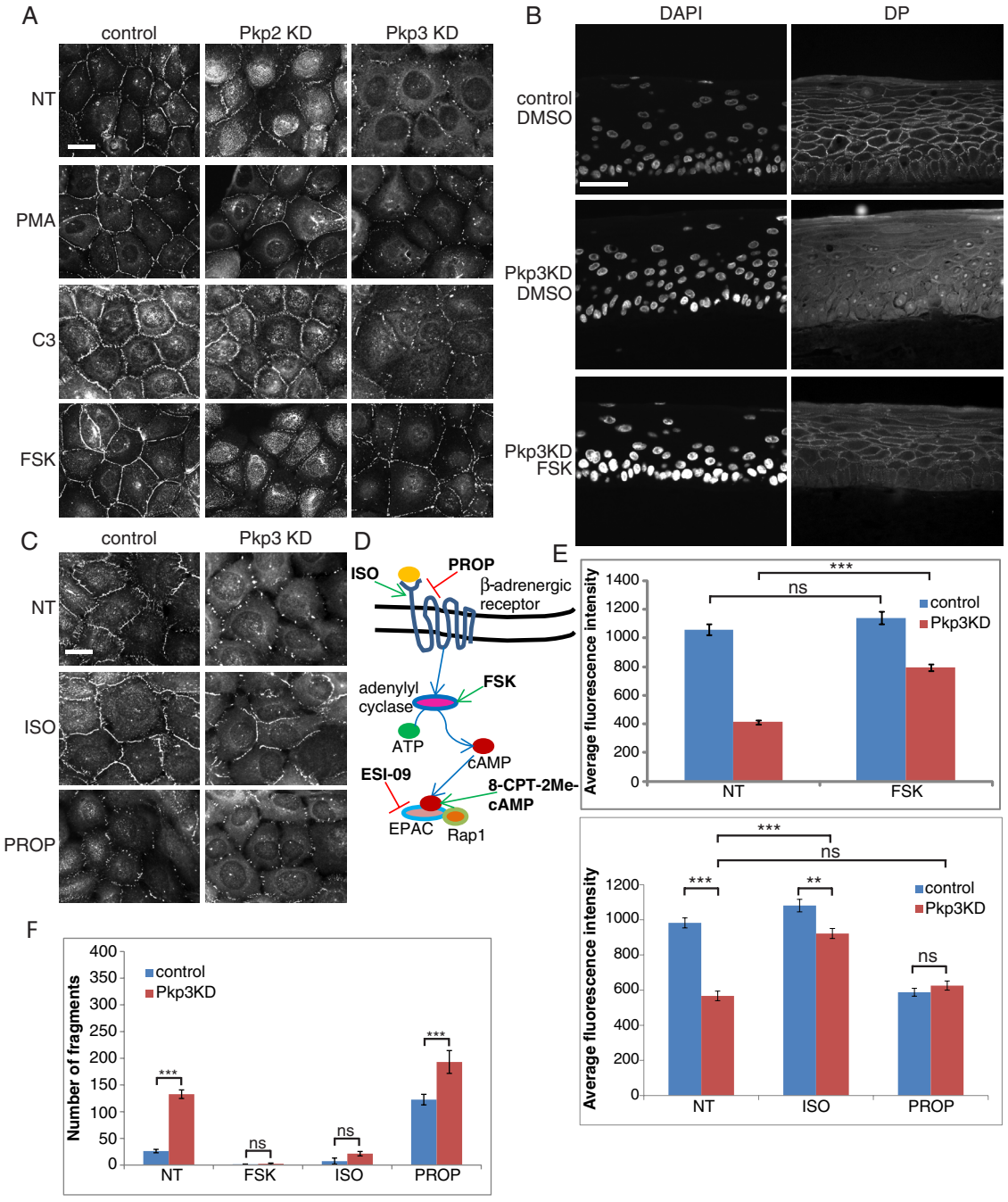

FIGURE 5: Activation of cAMP pathway reverses effects of Pkp3 ablation on desmosomal assembly and adhesion strength. (A) Immunofluorescence staining showing the effects on DP border localization of a PKC activator (PMA) and a RhoA inhibitor (C3) in Pkp2 KD and adenylyl cyclase activator (FSK) in Pkp3 KD SCC9 cells. Scale bar, 20 μm. (B) Immunofluorescence staining of 3D raft cultures after 6 d of differentiation shows recovery in DP distribution in Pkp3 KD rafts upon FSK treatment. Scale bar, 50 μm. (C) Immunofluorescence analysis of DP distribution in control and Pkp3-deficient SCC9 cells treated with vehicle, adrenergic agonist (ISO), or adrenergic antagonist (PROP). Scale bar, 20 μm. Note the recovery in ISO-treated Pkp3 KD and disruption of DP in PROP-treated control cells. (D) Cartoon depicting cAMP signaling with the activators and inhibitors used in this work. (E) Average fluorescence pixel intensities of DP at cell–cell borders of control and Pkp3 KD cells treated as specified in A (top, FSK) and C (bottom, ISO, PROP). Bars represent mean ± SEM. ns, $p > 0.05$, **$0.001 < p < 0.01$, ***$p < 0.001$ (ANOVA, Bonferroni). (F) Cell–cell adhesion strength assay demonstrating recovery of adhesion strength in Pkp3-ablated cells treated by FSK and ISO, as well as disruption of the adhesion strength in PROP-treated cells. Bars represent mean ± SEM. ns, $p > 0.05$, ***$p < 0.001$ (ANOVA, Bonferroni).

Intriguingly, the data also show that E-cad, a known functional interactor of Rap1 (Retta *et al.*, 2006; Li *et al.*, 2010), loses its ability to complex with Rap1 upon Pkp3 ablation. Further, in contrast to the largely distinct localization of E-cad and DP, E-cad and Pkp3 substantially colocalize at cell–cell borders, with a concentration of co-localizing signals at the cell margins (Figure 7C). E-cad knockdown

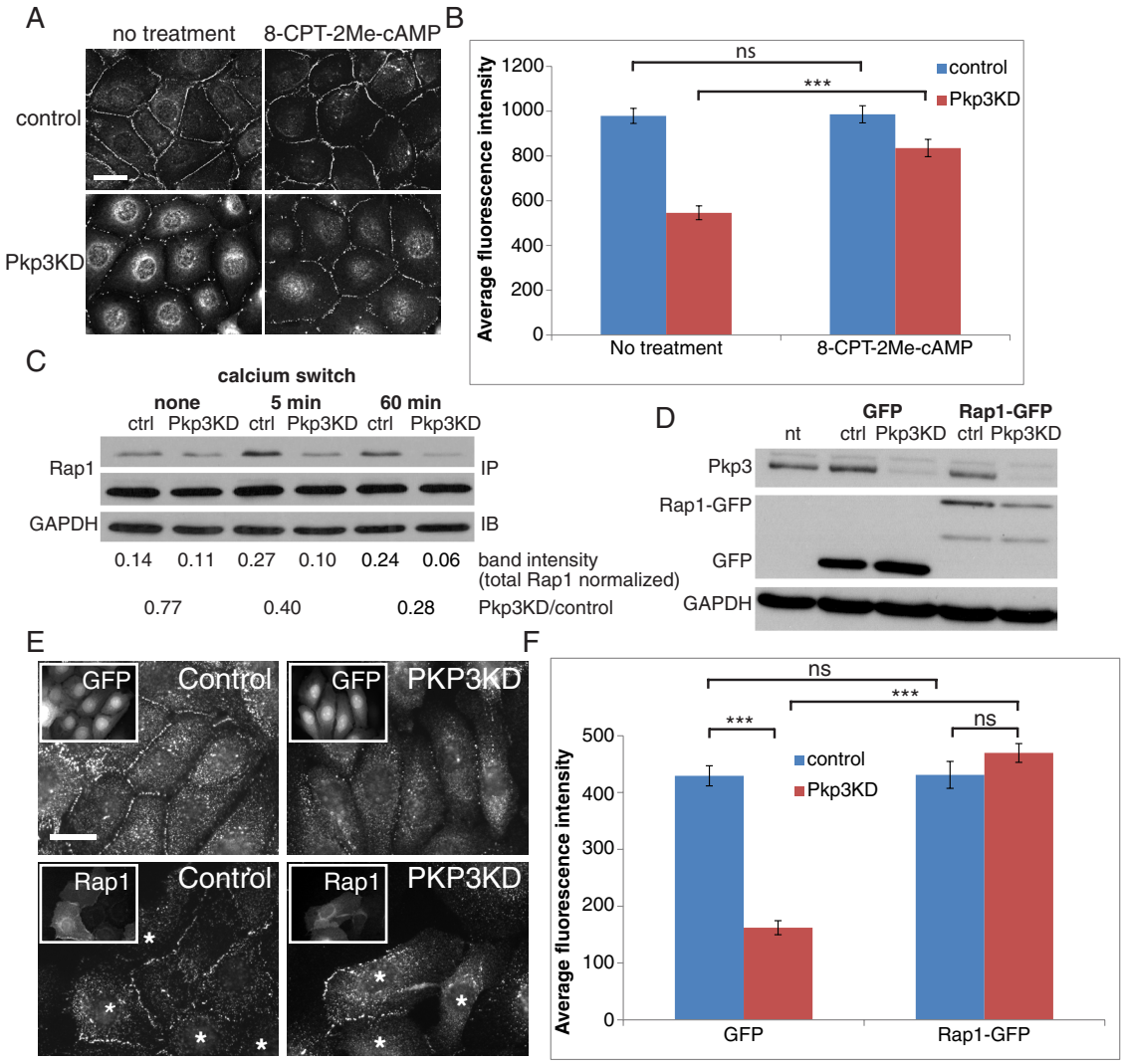

FIGURE 6: Pkp3-dependent Rap1 activation is required for normal DP border localization. (A) Immunofluorescence staining showing the effects of EPAC activator (8-CPT-2Me-cAMP) treatment on DP border localization in control and Pkp3 KD SCC9 cells. Scale bar, 20 μm. (B) Average DP border intensity for experiments in A. Bars represent mean ± SEM. ns, $p > 0.05$; ***$p < 0.001$ (ANOVA, Bonferroni). (C) Western blot showing the levels of GTP-bound (active) Rap1 in NHEK cells treated as indicated. Active Rap1 was pulled down using GST-RalGDS. Rap1 pull-down bands were normalized to total Rap1 using ImageJ. Ratio between activated Rap1 in control and Pkp3 KD cells shows a lack of increase in active Rap1 in Pkp3 KD cells upon calcium switch at 5 and 60 min. (D) Western blot showing the ectopic expression of GFP-tagged Rap1a in SCC9 cells compared with GFP-only control plasmid. nt, no transfection. (E) Immunofluorescence staining of DP showing the recovery of DP at the borders of Rap1-GFP– transfected Pkp3 KD cells. Note the lack of recovery in GFP-only cells. GFP and Rap1-GFP transfection efficiency is shown in the insets marked with white rectangles. Stars represent the cells that are GFP positive in the corresponding inset. Scale bar, 20 μm. (F) Average pixel intensities of DP at the borders of the cells in E. Bars represent mean ± SEM. ns, $p > 0.05$, ***$p < 0.001$ (ANOVA, Bonferroni).

did not have the same disruptive effect on Pkp3-Rap1 interaction or the interaction between Rap1 and its main activator, EPAC, suggesting that Pkp3 is required for Rap1 interaction with E-cad, but E-cad is not required for Pkp3-Rap1 interaction (Figure 7D). To test whether the activity of the Rap1 GEF EPAC was required for the maintenance of a Rap1/Pkp3/E-cad complex, we inhibited EPAC activity by using its well-established chemical inhibitor ESI-09 (Almahariq *et al.*, 2013). In the absence of EPAC activity, E-cad is excluded from a complex that still contains Pkp3 and Rap1, supporting the idea that Pkp3 provides a scaffold for binding and activation of Rap1 required for E-cad association (Figure 7E).

Pkp3 governs E-cad maturation

Because functional interactions between E-cad and Rap1 are critical for the formation of E-cad–based cell–cell junctions (Hogan *et al.*, 2004; Price *et al.*, 2004), we next tested whether Pkp3-deficient cells exhibited altered E-cad distribution at cell–cell borders. In cultures of SCC9 and HaCaT cells maintained in high calcium, E-cad membrane staining appeared less well-sealed compared with controls. Particularly in regions with the most aberrant DP, neighboring cells were connected by filopodial-like projections, sometimes with separation between adjacent cells, consistent with a failure to seal properly (Vasioukhin *et al.*, 2000; Figure 8 and Supplemental Figure S4).

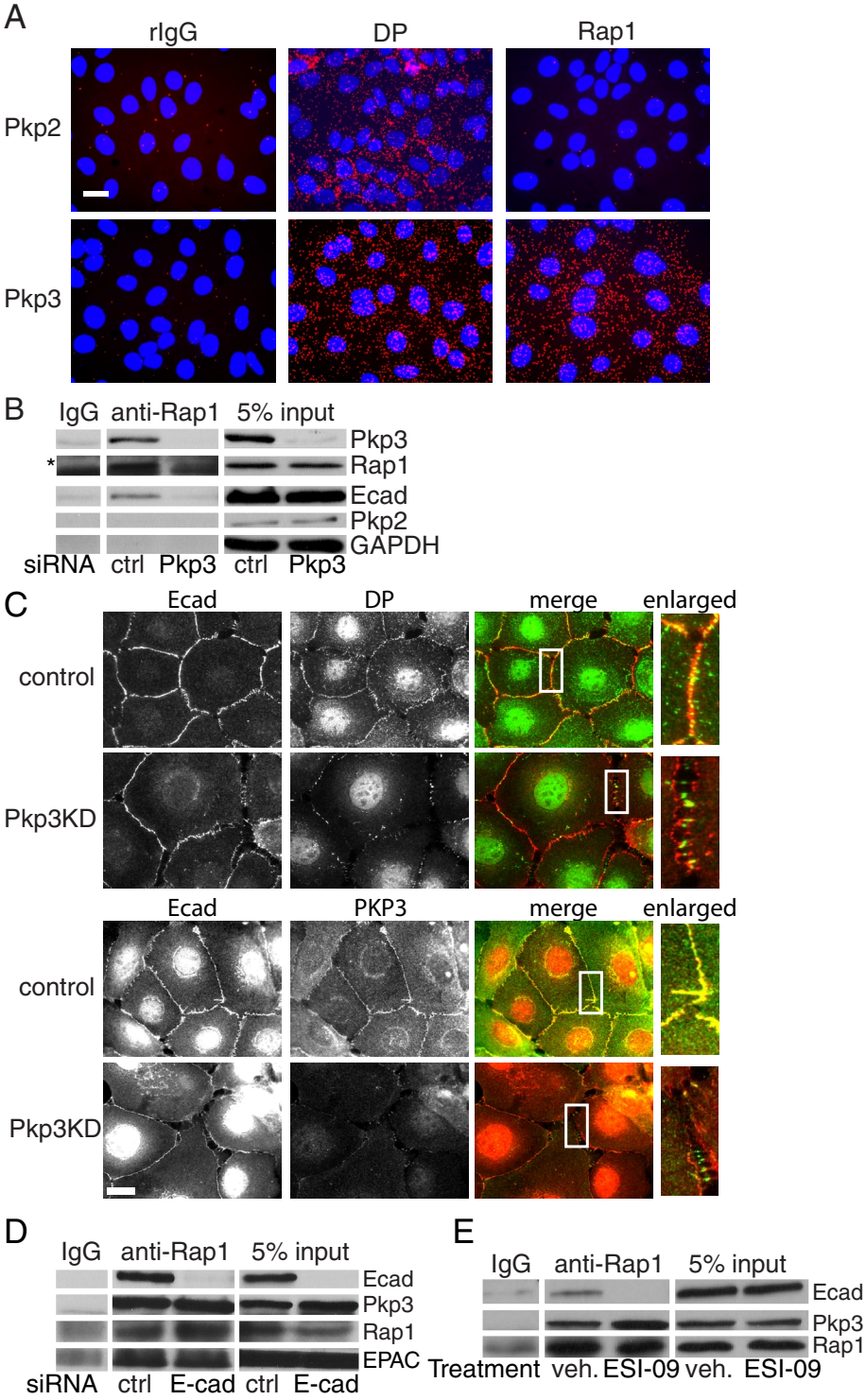

FIGURE 7: Pkp3-Rap1 complex is required for maintaining physical interaction between Rap1 and E-cad. (A) PLA (red dots) showing which of the molecular pairs indicated are in close proximity (within 100-nm range) within cells. Scale bar, 20 μm. (B) Western blot showing the immunoprecipitation (left) and total (right) protein levels of Pkp3, Rap1, E-cad, and Pkp2 for indicated conditions (with GAPDH as 5% loading control; asterisk indicates the Rap1 band just above the IgG light chain). Note the loss of E-cad from Rap1 complexes in Pkp3 KD condition. (C) Immunofluorescence staining showing the cell–cell border localization of E-cad in relation to DP (top) and Pkp3 (bottom). Note the minimal overlap between DP and E-cad and a substantial overlap between E-cad and Pkp3. Scale bar, 20 μm. (D) Western blot showing the immunoprecipitation (left) and total (right) protein levels of E-cad, Pkp3, Rap1, and EPAC for indicated conditions. Note that E-cad loss does not interfere with the interaction between Pkp3, Rap1, and EPAC. (E) Western blot showing the immunoprecipitation (left) and total (right) protein levels of E-cad, Pkp3, and Rap1 for indicated conditions. Note that the EPAC inhibitor ESI-09 causes the loss of E-cad but not Pkp3 from the Rap1 complex.

This pattern of E-cad was also observed in the dynamic conditions of calcium switch (Figure 8B). We further tested whether the cAMP pathway is involved in Pkp3-dependent E-cad distribution. Treatment of Pkp3KD cells with FSK reverses the E-cad phenotype, whereas inhibiting cAMP production with PROP results in an E-cad pattern similar to that seen in untreated Pkp3KD cells (Figure 8C), suggesting that Pkp3 regulates adherens junctions through cAMP-dependent signaling.

DISCUSSION

Although the general importance of Arm family members in desmosome and adherens junction function has been well established, we do not understand why multiple members of the plakophilin subfamily exist or the extent to which they have overlapping or specific functions. Here we establish Pkp3 as a critical component in desmosome assembly and cell–cell adhesion maintenance through a novel association with, and regulation of, Rap1. Pkp3 is also required for Rap1/E-cad interactions, as well as for E-cad maturation at sites of cell contacts. Our previous findings show that Pkp2 scaffolds PKCα and RhoA required for movement of DP precursor particles toward the sites of cell–cell contacts (Bass-Zubek *et al.*, 2008; Godsel *et al.*, 2010). In a similar manner, through its functional interactions with Rap1, Pkp3 may assist in the spatial and temporal coordination of adherens junction and desmosome assembly and maturation. This suggests that plakophilins are signaling specific scaffolds (Bass-Zubek *et al.*, 2009; Clevers and Nusse, 2012; Pieters *et al.*, 2012; Swope *et al.*, 2013) that ensure the correct positioning of their functional interactors required for coordination of cell–cell junction assembly.

Plakophilins are closely related, with Pkp3 sharing 51 and 51.9% similarity in Arm repeats and 44.3 and 44.9% overall homology with Pkp1 and Pkp2, respectively (Bonne *et al.*, 1999). In addition, there is significant overlap in their distribution among epithelial, heart, and neural tissues in species from *Xenopus* to human (Heid *et al.*, 1994; Mertens *et al.*, 1996; Moll *et al.*, 1997; Schmidt *et al.*, 1999). Further, substantial compensatory overexpression of Pkp1 was

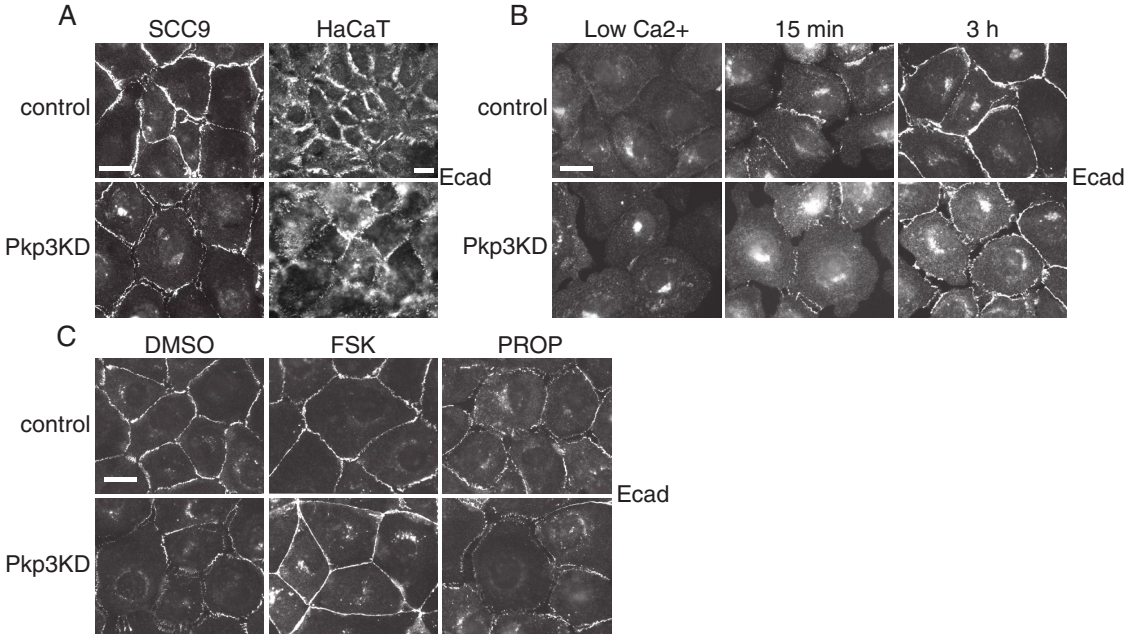

FIGURE 8: Pkp3 deficiency causes defects in cAMP-dependent E-cad maturation. (A) Immunofluorescence staining of E-cad in SCC9 (left) and HaCaT (right) cells shows aberrant cell–cell junction localization in steady-state high-calcium conditions in Pkp3KD cells compared with the control. (B) Immunofluorescence staining showing a defect in maturation of E-cad upon calcium switch at the sites of cell–cell contact in the Pkp3 KD SCC9 cells compared with control. (C) Immunofluorescence staining showing the recovery of E-cad at the borders of Pkp3 KD cells treated with forskolin. Conversely, control cells treated with propranolol mimic the immature appearance of E-cad junctions in a manner similar to the Pkp3 KD cells. Scale bars, 20 μm.

observed in Pkp3-knockout mice (Sklyarova *et al.*, 2008), which may have ameliorated some of the effects of Pkp3 ablation. Together these data raise the question of the extent to which there is functional overlap among the Pkp family members.

Here we addressed the problem of compensatory overexpression by using two distinct model systems. In our two-dimensional experimental model system (SCC9, A431, and HaCaT cells), Pkp1 is not expressed, and no compensatory up-regulation of other plakophilins is observable upon either Pkp2 or Pkp3 silencing (Figure 1). This makes the model particularly suitable for determining which functions are shared (recruitment of DP to nascent sites of cell–cell contact during the initial phase of assembly) by Pkp2 and Pkp3 and which are specific (scaffolding of the distinct molecular complexes required for the later phases of desmosome assembly). Of importance, despite the presence of normal levels of Pkp1 and 2 (Supplemental Figure S1G), the 3D organotypic model system of developing epidermis recapitulates the cAMP-dependent loss of DP at the cell–cell borders in Pkp3-silenced rafts (Figures 2 and 5). The inability of other plakophilins present in the organotypic model (especially Pkp1, whose overexpression partially compensated for Pkp3 loss in mice; Sklyarova *et al.*, 2008) to take over the role of Pkp3 in desmosome assembly demonstrates the specificity of its functions.

The differences in phenotypes of Pkp2 and Pkp3 KD cells suggest that, despite some redundant roles, plakophilins serve as scaffolds for specific signaling molecules. In this role they regulate spatiotemporal distribution as well as the activity status of the signaling complexes they tether in order to accomplish cell–cell junction assembly and maintenance. We show here that Pkp2 and 3 differ in the signaling partners they harness, as well as in the phase of desmosome assembly they regulate. Whereas Pkp3-dependent activation of Rap1 is required for formation of DP-containing desmosome precursors in the cytoplasm as well as size stabilization of nascent desmosomes, Pkp2 helps to transfer already formed precursors from the cytoplasm to sites of cell–cell contacts by harnessing PKC and RhoA activity (Figures 2–6 and see later discussion of Figure 9; Bass-Zubek *et al.*, 2008; Godsel *et al.*, 2010). Therefore Pkp3 ablation leads to an apparent loss of cytoplasmic desmosome precursors, precluding phases 2 and 3 of desmosome assembly. On the other hand, Pkp2 silencing affects only the ultimate phase of the assembly by preventing the transport of the formed precursors to the membrane. The ablation of both Pkps results in failure of phase 1, as no DP is observed at the sites of cell–cell contact (Figure 2).

Our previous work in cells treated with either FSK or PKC activators suggested that DP assembly and accumulation in junctions may be regulated by adenylyl cyclase and PKCα (Stappenbeck *et al.*, 1994; Godsel *et al.*, 2005). However, whereas PKCα has been shown to regulate DP stability and internalization (Kroger *et al.*, 2013), PKA-dependent effects on DP and desmosomes have not yet been established (Supplemental Figure S3). Moreover, studies on Pkp2 and its role in DP localization and desmosome assembly did not find a link between this plakophilin and cAMP-dependent PKA (Bass-Zubek *et al.*, 2008), establishing Pkp2 instead as a PKCα and RhoA signaling scaffold (Bass-Zubek *et al.*, 2008; Godsel *et al.*, 2010). Here we show that global chemical activation and inhibition of PKCα and RhoA pathways, respectively (Figure 5), while able to restore normal DP localization in Pkp2 KD cells, were unable to do so in Pkp3 KD cells. Instead, we show that activating the cAMP-dependent EPAC-Rap1 pathway rescued desmosome assembly in Pkp3-deficient cells, with no effect on Pkp2 KD (Figures 5 and 6). Collectively these results suggest that when the concentration of signaling mediators is low, Pkp2 and Pkp3 are required to bring PKCα, RhoA, and EPAC/Rap1 in the proximity of their targets. However, global activation of these signaling molecules circumvents the need for their scaffolding activity, thereby rescuing Pkp2 and 3 ablation phenotypes.

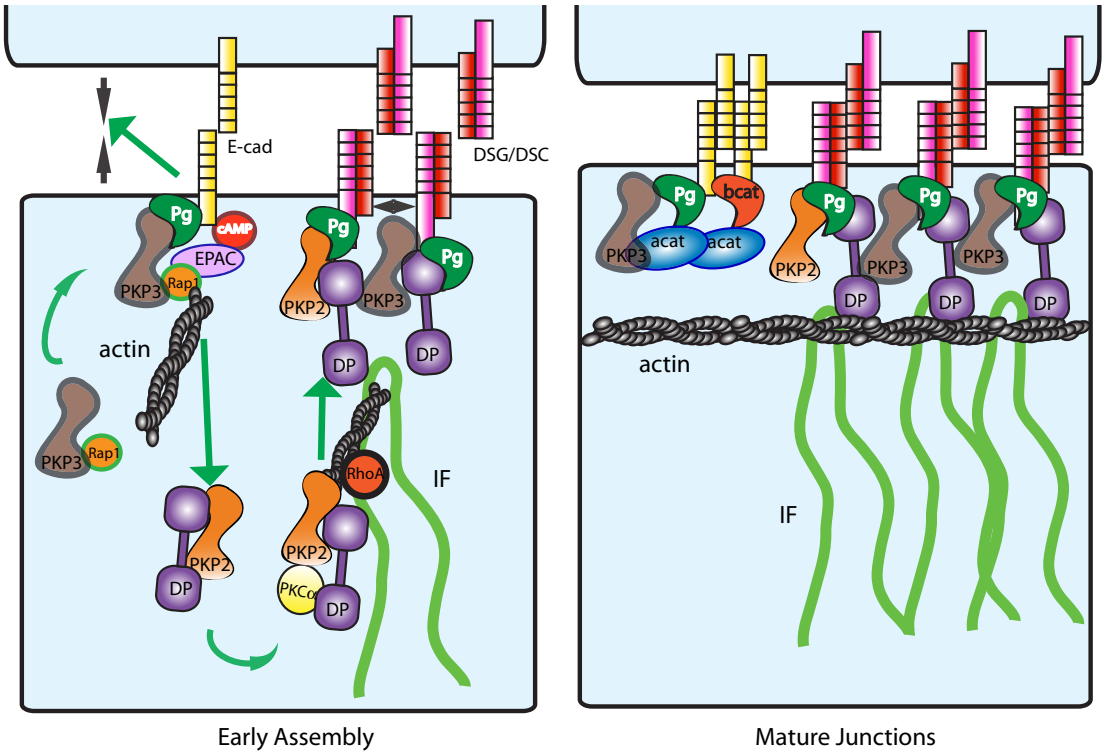

FIGURE 9: Model for the role of Pkp3 in cell–cell junction formation. Left, activation of cAMP pathway upon cell–cell contact in high calcium leads to rapid recruitment of Pkp3-Rap1 complex to E-cad. At the same time, juxtamembrane DP coalesces at the sites of cell–cell contacts, requiring either Pkp2 or Pkp3, forming nascent desmosomes. Functional Pkp3-Rap1-E-cad complex drives adherens junction maturation by pulling the cells closer together and desmosome assembly by signaling the formation of cytoplasmic DP particles. On the other hand, Pkp3 acts as a spacer, preventing the aberrant coalescence of nascent desmosomes at the membrane. Pkp2 harnesses the activity of PKCα and RhoA to facilitate actin-dependent transport of cytoplasmic DP particles to the membrane. Right, model of steady-state adherens and desmosome junctions demonstrating mature cortical actin distribution and correctly sealed adherens junctions in the presence of Pkp3. In the absence of Pkp3 (not shown), Pkp3-Rap1-E-cad complex fails to assemble, leading to immature adherens junctions and failure of DP cytoplasmic particles to form. In addition, aberrant coalescence of nascent desmosomes occurs at the membrane.

Rap1 GTPase is an immediate downstream target of EPAC (de Rooij *et al.*, 1998), an important factor for proper adherens junction assembly (Boettner and Van Aelst, 2009; Wittchen and Hartnett, 2011). Because Rap1 supports E-cad junctional maintenance through support of E-cad–mediated cell–cell adhesion (Price *et al.*, 2004) and inhibition of E-cad endocytosis (Hoshino *et al.*, 2005), we tested whether E-cad/Rap1 interaction was disrupted in Pkp3 KD cells. Indeed, Pkp3 ablation caused disruption of E-cad/Rap1 interactions, whereas ablation of E-cad failed to disrupt the Pkp3/Rap1 complex (Figure 7). This suggests that Pkp3 is involved in adherens junction assembly and maintenance through its regulation of Rap1 activity and Rap1 interaction with E-cad. Unlike functional disruption of other desmosomal components, such as Pkp2 (Bass-Zubek *et al.*, 2008; Godsel *et al.*, 2010), Pg (Yin *et al.*, 2005), and Dsg 1 (Simpson *et al.*, 2010a), which leave E-cad border localization intact, Pkp3 ablation caused changes in E-cad border appearance (Figure 8). These changes, which appeared early during junction assembly and persisted in steady-state conditions, were consistent with the idea that E-cad–based junctions do not undergo proper sealing and maturation (Supplemental Figure S4; Vasioukhin *et al.*, 2000). Moreover, these changes were partially reversed by hyperactivation of the cAMP pathway (Figure 8). A report suggested that E-cad and Pg recruit Pkp3 to the cell–cell border in order to initiate desmosome assembly (Gosavi *et al.*, 2011), thus opening the possibility of a two-way regulatory loop between E-cad and Pkp3. E-cad recruits Pkp3 to the sites of cell–cell adhesion, whereas Pkp3 would bring Rap1 to complex with E-cad as required for adherens junction maturation (Figure 9). Adherens junctions have been reported to provide structural and signaling cues that initiate desmosome assembly (O'Keefe *et al.*, 1987; Lewis *et al.*, 1997). Thus it is plausible that Pkp3-mediated E-cad interaction with Rap1 initializes the assembly of the desmosomal precursors in the cytoplasm (Figure 9). In addition, this complex may be responsible for nascent desmosome stabilization at the sites of cell–cell contact. However, Pkp3 may regulate desmosome assembly independently from E-cad/Rap1 signaling. In either of these two scenarios, Pkp3-dependent regulation of Rap1 is required for the correct assembly of mature desmosomal and classic cadherin-based intercellular junctions.

Mutations in Pkp1 and 2 result in ectodermal dysplasia-skin fragility syndrome (McGrath and Mellerio, 2010) and arrhythmogenic right ventricular cardiomyopathy (Rickelt and Pieperhoff, 2012), respectively. Loss of Pkp3 has been associated with several types of cancer (Furukawa *et al.*, 2005; Aigner *et al.*, 2007; Valladares-Ayerbes *et al.*, 2008, 2010; Takahashi *et al.*, 2012). The extent to which these diseases are caused by the failure of the common adhesive functions shared by all plakophilins or the disruption of specific signaling mediators is unknown. Considering their distinct tissue and differentiation expression patterns (as discussed earlier), as well

as different and dynamic intracellular localization (Bonne *et al.*, 1999; Mertens *et al.*, 2001; Sobolik-Delmaire *et al.*, 2010), it is tempting to speculate that interference with Pkp-scaffolded signaling effectors is an important contributing factor. Consistent with this idea, a study in a mouse model of the autoimmune skin blistering disease pemphigus vulgaris (PV) reported a potential role for cAMP signaling in preserving barrier function and skin mechanical integrity (Spindler *et al.*, 2010). Moreover, binding of PV immunoglobulin G (IgG) to keratinocyte cell surfaces causes rapid Pkp3 phosphorylation, detachment from its binding partner Dsg3, and accumulation in the cytoplasm (Cirillo *et al.*, 2013). Our data identify Pkp3 as a molecular regulator of cAMP-dependent activity of Rap1. It will be interesting to see whether Pkp3 and Rap1 are affected in blistering diseases with potential cAMP involvement. Therefore finding new functional partners for all three plakophilin family members may help with diagnosis and development of therapeutic interventions for desmosome-related diseases (D'Alessandro *et al.*, 2012; Tsuruta *et al.*, 2012).

MATERIALS AND METHODS

DNA constructs and siRNA

GFP-tagged human Pkp3 retroviral constructs in pLZBob vector were a gift from J. Wahl (University of Nebraska Medical Center, Omaha, NE). GFP-tagged human wild-type Rap1a in pEGFP-C1 vector was a gift from C. Niessen (University of Cologne, Cologne, Germany). The DP.GFP construct and the inducible expressing cells used in live-cell imaging experiments have been described previously (Godsel *et al.*, 2005). Pooled and individual sequences of siRNAs against a nontargeting control, Pkp2 (for sequences see Koetsier *et al.*, 2013), and Pkp3 were obtained from Thermo Fisher Scientific (Lafayette, CO; open reading frame targeting sequences: [1] 5′-GAUCUGAGCUGCAGUCGGA-3′; [2] 5′-ACAACAAGCUCCACCGUGA-3′; [4] 5′-GGGCGAAGGGCUAUCGGAA-3′; and [17] 5′-GGGUUCAACAGCUACGGUA-3′) and Integrated DNA Technologies (Coralville, IA; 5′-untranslated region targeting duplex: [S] 5′-GGGACAGGACGUGAAGAUAGUUGGG-3′ and [AS] 5′-CCCAACUAUCUUCACGUCCUGUCCCUC-3′).

Cell lines and transfections

SCC9 (a gift from L. Hudson, University of New Mexico, Albuquerque, NM), HaCaT, and A431 cells were maintained in DMEM/F-12 and DMEM, respectively, supplemented with 10% fetal bovine serum (FBS) and 1% penicillin/streptomycin and grown at 37°C in 5% CO_2. Normal human keratinocytes (NHEKs) were obtained from the Northwestern University Skin Disease Research Center (Chicago, IL) and isolated from neonatal foreskins as previously described (Halbert *et al.*, 1992). NHEKs were grown in medium 154 containing human keratinocyte growth supplement, gentamicin/amphotericin B solution (Invitrogen, Carlsbad, CA), and 0.07 mM $CaCl_2$. siRNAs were transfected using Dharmafect1 reagent (Thermo Fisher Scientific) following the manufacturer's instructions, with a final siRNA concentration of 20 nM used throughout. In some experiments, NHEKs and SCC9s were transfected with siRNAs and plasmids by AMAXA nucleoporation (Lonza, Walkersville, MD) according to manufacturer's instructions.

3D organotypic keratinocyte raft cultures

For stratified, 3D keratinocyte cultures, cells were expanded and siRNAs were introduced using AMAXA electroporation. Cells were then seeded on collagen plugs and grown at an air–medium interface according to published protocols (Simpson *et al.*, 2010b). These air-lifted cultures were grown for 6 d. Rafts were either lysed for protein analysis or fixed in 10% neutral-buffered Formalin to be processed for paraffin embedding. For some experiments, raft cultures were electroporated as described and then treated with dimethyl sulfoxide (Thermo Fisher Scientific) or 100 μM forskolin (Sigma-Aldrich, St. Louis, MO) 48 h before harvesting.

Calcium switch treatments

SCC9 and A431 cells were incubated in low-calcium medium (DMEM with 0.05 mM $CaCl_2$) for 16–24 h and then switched to their respective normal growth media containing >1.8 mM Ca^{2+} to induce cell–cell junction assembly (Godsel *et al.*, 2010). For analysis of cell–cell contact–induced desmosome formation in NHEKs, calcium switch was performed by switching cells to medium 154 containing 1.2 mM Ca^{2+} for 6 h.

Antibodies and chemical reagents

The following mouse antibodies were used: anti-Pkp2 (Progen Biotechnik, Heidelberg, Germany); 23E3, anti-Pkp3 (Invitrogen); anti-P0071(Pkp4) (Acris Antibodies, Herford, Germany); 11F5, anti-DP (gift from David Garrod, University of Manchester, Manchester, United Kingdom); 12G10, anti-tubulin (provided by J. Frankel and E. M. Nelson from the Developmental Studies Hybridoma Bank, University of Iowa, Iowa City, IA); 6D8, anti-Dsg2; 7G6, anti-Dsc2 (gifts from J. Wahl); and HECD-1, anti–E-cad (gift from M. Takeichi and O. Abe, University of Tokyo, Tokyo, Japan; Shimoyama *et al.*, 1989). The following rabbit antibodies were used: 667, anti-PKP1 (gift from M. Hatzfeld, Martin Luther University Halle, Halle, Germany); C2206, anti–β-catenin (Sigma-Aldrich); anti–glyceraldehyde-3-phosphate dehydrogenase (GAPDH; Sigma-Aldrich); NW6, anti-DP (Angst *et al.*, 1990); and anti-Rap1 (Abcam, Cambridge, MA). One chicken antibody was used: 1407, anti-PG antibody (Aves Labs, Tigard, OR). For inhibition and activation of adenylyl cyclase- and cAMP-dependent EPAC-Rap1, PKCα, and RhoA, media were supplemented with forskolin (100 μM), isoprenaline (10 μM), propranolol (10 μM), 8-CTP-2Me-cAMP (10 μM), ESI-09 (5 μM), PMA (100 nM) (all from Sigma-Aldrich), or C3 transferase-based RhoA inhibitor (1 μM; Cytoskeleton, Denver, CO) and were used with appropriate vehicle control.

Electron microscopy

Cells were grown on Thermanox coverslips (VWR, Pittsburgh, PA). Preparation of the cells for electron microscopy and the electron microscopy were done in collaboration with the Northwestern University Cell Imaging Facility. The monolayers were fixed in 2.0% paraformaldehyde/2.5% gluteraldehyde in 0.1 M sodium cacodylate, pH 7.4, for 30 min at room temperature. They were refixed in 2% osmium tetroxide for 30 min and 3% uranyl acetate for 90 min. Samples were dehydrated in a series: a duplication of 50, 70, 80, 90, and three times in 100% ethyl alcohol. Afterward they were embedded in Epon embedding resin mixture. Sample blocks were sectioned at 70-nm thickness using Leica EM UC6 (Buffalo Grove, IL). Sections were collected onto copper grids and counterstained in 3% uranyl acetate and lead citrate. Images were taken on a Tecnai Spirit G2 TEM (FEI, Hillsborough, OR) using TIA imaging application software.

Immunohistochemistry, immunofluorescence, and image acquisition and analysis

Raft cultures were sectioned and processed for immunohistochemical staining using conventional methods. Antigen retrieval was performed by heating to 95°C in 0.01 M citrate buffer containing 0.05% Tween-20. Sections were blocked in 10% normal goat serum (Jackson Labs, West Grove, PA) for 60 min at 37°C, incubated in

primary antibody in 0.5% bovine serum albumin (BSA) overnight at 4°C, incubated in fluorophore-linked secondary antibody in 0.5% BSA for 60 min at 37°C, and mounted in polyvinyl alcohol. For immunofluorescence, cells grown on glass coverslips were fixed in ice-cold methanol for 2 min. Primary and secondary antibody incubations were performed at room temperature for 1 h, interspaced by multiple washes in phosphate-buffered saline (PBS), followed by mounting of the coverslips with polyvinyl alcohol (Sigma-Aldrich) containing 4′,6-diamidino-2-phenylindole to counterstain the nuclei (Sigma-Aldrich). Fixed cells were visualized with a Leica microscope (DMR) fitted with a 63× objective (PL APO, numerical aperture [NA], 1.32). Images were captured with an Orca 100 charge-coupled device camera (C4742-95; Hamamatsu, Bridgewater, NJ) and MetaMorph V7.7.0.0 imaging software (Molecular Devices, Sunnyvale, CA). Images in Supplemental Figure S4 were captured with a Zeiss Axio Imager.Z1 microscope fitted with a 63× objective (Plan Apochromat; NA 1.4) and an Axiocam MRm camera using Zeiss AxioVision 4.8.2 software. Fluorescence DP border pixel intensity was measured and calculated using MetaMorph 7.7. Average background intensity measured at the cell-free areas was subtracted from border intensity. At least 100 individual borders were measured per condition, with error bars representing SEM. All experiments were performed in at least three independent replicates.

Time-lapse imaging of fluorescently tagged desmoplakin

For live imaging, 3 d after transfection, PKP3 siRNA– and control-transfected DP-GFP– expressing cells were seeded onto LabTek chambered coverglass slides (Thermo Fisher Scientific). Cell monolayers were wounded with a 26-gauge needle and incubated in imaging medium (Hanks' balanced salt solution, 20 mM 4-(2-hydroxyethyl)-1-piperazineethanesulfonic acid, 1% FBS, 2 mM L-glutamine, 4.5 g/l glucose, and 1× amino acids) at 37°C for 60 min and then processed for time-lapse imaging. DP-GFP fluorescence time-lapse recordings for particle analysis were obtained at consistent time intervals of 5 min with rapid *z*-stack acquisition (5–7 planes; 1-µm step size) using an Application Solution Multidimensional Workstation (Leica), an inverted microscope (DMIRE2; Leica) fitted with a CoolSNAP HQ camera (Roper Scientific, Tucson, AZ), and a 63× objective (HCX PL APO, glycerine, NA 1.3) with a piezo element. Cells were subjected to imaging in a 37°C climate chamber. Fluorescent DP particle analysis was conducted by MetaMorph 7.7. For supplemental videos we recorded DP-GFP fluorescent particles at consistent 1-min intervals with *z*-stack acquisition (5–7 planes; 0.25-µm step size). Time-lapse images were captured using a DM16000 (Leica Microsystems) within a 37°C environmental control system chamber using 100-W mercury halide fiber optic illumination with 63× objective (HCX PL APO, NA 1.4) and an ORCA-ER AG camera. Images were captured using Simple PCI version 6.0 (Hamamatsu). All images were processed using a true 3D fixed PSF deconvolution synthetic algorithm (20 iterations) contained within the AutoQuantX X2.2.1 software (MediaCybernetics, Bethesda MD), and single-plane images were cropped, brightened, and contrasted using MetaMorph V7.7.0.0 imaging software (Molecular Devices) and compressed and compiled into QuickTime videos with ImageJ 1.44p software (National Institutes of Health, Bethesda, MD).

cAMP measurement

To measure the intracellular concentration of cAMP, we used an enzyme-linked immunosorbent assay–based cAMP Enzyme Immunoassay Kit (Sigma-Aldrich) according to the manufacturer's protocol for acetylated samples. The staining intensity corresponding to cAMP levels was determined at 405-nm wavelength using a Synergy 2 plate reader (Biotek, Winooski, VT).

Purification of recombinant RalGDS and rap1 activity pull downs

Glutathione *S*-transferase (GST)-RalGDS-RBD–expressing vector was a gift from Keith Burridge (University of North Carolina, Chapel Hill, NC). Purification of RalGDS and activated Rap1 pull downs were performed as previously described (van Triest *et al.*, 2001). The bacterial lysate from cells expressing GST-RalGDS-RBD was collected in modified RIPA buffer (50 mM Tris, pH 7.6, 50 mM NaCl, 5 mM $MgCl_2$, 1% Triton X-100, 1 mM dithiothreitol, and protease inhibitors [Complete; Roche Diagnostics, Indianapolis, IN]) and incubated with glutathione Sepharose 4B beads (GE Healthcare, Piscataway, NJ) for 1 h at 4°C, followed by several washes in lysis buffer. For GTPase pull downs, cells were lysed in 50 mM Tris (pH 7.6), 500 mM NaCl, 1% Triton X-100, 0.1% SDS, 0.5% deoxycholate, 10 mM $MgCl_2$, and protease inhibitors. Lysates were clarified by centrifugation, equalized for total protein concentration, and incubated with 50–100 µg of GST-RalGDS-RBD–bound Sepharose beads for 30 min at 4°C. Beads were washed in modified RIPA buffer and further processed for SDS–PAGE and Western blotting.

Western blotting and saponin solubility assay

To analyze protein expression, cells were washed briefly in PBS and lysed in urea sample buffer (8 M deionized urea, 1% SDS, 10% glycerol, 60 mM Tris, pH 6.8, and 5% β-mercaptoethanol) and equalized. Samples were subjected to SDS–PAGE electrophoresis on 7.5 or 15% polyacrylamide gels followed by transfer to polyvinylidene fluoride (EMD-Millipore, Billerica, MA) or nitrocellulose membranes (VWR). Membranes were probed with specific primary and secondary antibodies and visualized using enhanced chemiluminescence and x-ray film (Denville, Metuchen, NJ). Western blots were quantified by standard densitometry analysis using ImageJ software. All blots shown are representative data obtained from three independent experiments. Saponin extraction was used for analysis of cytosolic proteins. Cells were lysed for 10 min on ice in saponin buffer (10 mM Tris, pH 7.5, 140 mM NaCl, 0.01% saponin, 5 mM EDTA, 2 mM ethylene glycol tetraacetic acid [EGTA], and protease inhibitors), followed by centrifugation at 22,000 rcf at 4°C for 30 min. Supernatant was used to determine the cytosolic protein fraction, and saponin-insoluble pellet was solubilized in urea sample buffer and resolved on Western blot.

Coimmunoprecipitation

Coimmunoprecipitation was performed by lysing cells in an IP lysis buffer (10 mM Tris-HCl, pH 7.5, 0.5% Triton X-100, 145 mM NaCl, 10% glycerol, 5 mM EDTA, 2 mM EGTA) supplemented with an EDTA-free protease inhibitor tablets (Roche). Lysates were centrifuged at 22,000 rcf at 4°C for 30 min. Supernatants were incubated with 5 µl of anti-Rap1 or rabbit isotype control antibodies at 4°C for 2 h, and then 20 µl of GammaBind Sepharose (GE Healthcare) was added and incubated with rotation at 4°C for 30 min. Samples were washed three times with lysis buffer. The immune complexes were released by boiling the beads with reducing Laemmli buffer and further analyzed by Western blotting.

In situ proximity ligation assay

Cells were fixed with methanol, permeabilized with 0.2% Triton X-100, and blocked with 1% BSA and 10% goat serum in PBS. Samples were incubated overnight with rabbit–mouse antibody pairs as

indicated in the text describing each experiment. Ligation and amplification were executed following the manufacturer's manual (Duolink in Situ PLA; Olink Bioscience, Uppsala, Sweden), using the following reagents contained in the kit: PLA probe anti-rabbit plus, PLA probe anti-mouse minus, and detection reagent red. Fluorescence signals were visualized, and images were taken using a microscope (DSM; Leica) fitted with a 40× oil objective (PL Fluoratar, NA 1.0).

Cell–cell adhesion mechanical strength assay

Confluent siRNA-transfected SCC9 cells grown in six-well plates were washed with PBS and incubated with 2.4 U/ml dispase (Roche Diagnostics) for 30 min at 37°C. The released cell sheets were then exposed to equal amounts of sheer stress using an orbital Symphony microplate shaker (VWR) at 1000 rpm for 1 min until the cell sheets broke apart into fragments. The fragments were then imaged with a Hamamatsu Orca digital camera mounted on a MZ6 dissecting scope (Leica Microsystems) as described previously (Hudson *et al.*, 2004) and analyzed using MetaVue imaging software (Universal Imaging, Downingtown, PA). Under experimental conditions in which fragmentation was excessive, a maximum of 800 fragments was counted.

Data collection and statistical methods

All experiments were carried out in at least three independent biological replicates. Values are given as mean with error bars indicating SEM. Unpaired *t* tests with two-tailed *p* values and 95% confidence intervals were conducted for all experiments consisting of two experimental groups. For experiments consisting of three or more groups we used one-sided analysis of variance (ANOVA) with Bonferroni correction to compare selected pairs of means. In all cases, $p > 0.05$ was considered not significant (ns); $0.01 < p < 0.05$ was considered significant (*); $0.001 < p < 0.01$ was considered very significant (**); and $p < 0.001$ was considered extremely significant (***). All calculations were conducted using Prism software (GraphPad, San Diego, CA).

ACKNOWLEDGMENTS

This work was supported by National Institutes of Health Grant R37 AR43380 with additional support from AR041836 and CA122151 to K.J.G. from the J.L. Mayberry Endowment. L.M.G. was supported by a Dermatology Foundation Career Development Grant and the Skin Cancer Foundation Paul Silberberg. Imaging work performed at the Northwestern University Cell Imaging Facility was generously supported by Cancer Center Support Grant P30 CA060553 awarded to the Robert H. Lurie Comprehensive Cancer Center. Paul Hoover supplied primary keratinocyte cultures from the Northwestern University Skin Disease Research Center Keratinocyte Core Facility with support from the National Institutes of Health/National Institute of Arthritis and Musculoskeletal and Skin Diseases (5P30AR057216-02). Any opinions, findings, and conclusions or recommendations expressed in this material are those of the authors and do not necessarily reflect the views of the Northwestern University Skin Disease Research Center or the National Institutes of Health/National Institute of Arthritis and Musculoskeletal and Skin Diseases or National Cancer Institute. In addition, we thank Adi Dubash for technical advice on small GTPases, Volodya Gelfand and Caroline Hookway (Northwestern University, Chicago, IL) for helpful discussion and technical advice, and Spiro Getsios (Northwestern University, Chicago, IL) for the use of the Zeiss Axio Imager.Z1 microscope.

REFERENCES

Adams CL, Chen Y-T, Smith SJ, Nelson WJ (1998). Mechanisms of epithelial cell-cell adhesion and cell compaction revealed by high-resolution tracking of E-cadherin-green fluorescent protein. J Cell Biol 142, 1105–1119.

Aigner K, Descovich L, Mikula M, Sultan A, Dampier B, Bonne S, van Roy F, Mikulits W, Schreiber M, Brabletz T, *et al.* (2007). The transcription factor ZEB1 (deltaEF1) represses Plakophilin 3 during human cancer progression. FEBS Lett 581, 1617–1624.

Almahariq M, Tsalkova T, Mei FC, Chen H, Zhou J, Sastry SK, Schwede F, Cheng X (2013). A novel EPAC-specific inhibitor suppresses pancreatic cancer cell migration and invasion. Mol Pharmacol 83, 122–128.

Amagai M, Stanley JR (2012). Desmoglein as a target in skin disease and beyond. J Invest Dermatol 132, 776–784.

Angst BD, Nilles LA, Green KJ (1990). Desmoplakin II expression is not restricted to stratified epithelia. J Cell Sci 97, 247–257.

Bass-Zubek AE, Godsel LM, Delmar M, Green KJ (2009). Plakophilins: multifunctional scaffolds for adhesion and signaling. Curr Opin Cell Biol 21, 708–716.

Bass-Zubek AE, Hobbs RP, Amargo EV, Garcia NJ, Hsieh SN, Chen X, Wahl JK3rd, Denning MF, Green KJ (2008). Plakophilin 2: a critical scaffold for PKC alpha that regulates intercellular junction assembly. J Cell Biol 181, 605–613.

Boettner B, Van Aelst L (2009). Control of cell adhesion dynamics by Rap1 signaling. Curr Opin Cell Biol 21, 684–693.

Bonne S, Gilbert B, Hatzfeld M, Chen X, Green KJ, van Roy F (2003). Defining desmosomal plakophilin-3 interactions. J Cell Biol 161, 403–416.

Bonne S, van Hengel J, Nollet F, Kools P, van Roy F (1999). Plakophilin-3, a novel armadillo-like protein present in nuclei and desmosomes of epithelial cells. J Cell Sci 112, 2265–2276.

Campuzano O, Alcalde M, Allegue C, Iglesias A, Garcia-Pavia P, Partemi S, Oliva A, Pascali VL, Berne P, Sarquella-Brugada G, *et al.* (2013). Genetics of arrhythmogenic right ventricular cardiomyopathy. J Med Genet 50, 280–289.

Chen X, Bonne S, Hatzfeld M, van Roy F, Green KJ (2002). Protein binding and functional characterization of plakophilin 2. Evidence for its diverse roles in desmosomes and beta-catenin signaling. J Biol Chem 277, 10512–10522.

Cheng X, Ji Z, Tsalkova T, Mei F (2008). Epac and PKA: a tale of two intracellular cAMP receptors. Acta Biochim Biophys Sin 40, 651–662.

Cirillo N, Alshwaimi E, McCullough M, Prime SS (2013). Pemphigus vulgaris autoimmune globulin induces Src-dependent tyrosine-phosphorylation of plakophilin 3 and its detachment from desmoglein 3. Autoimmunity 47, 134–140.

Clevers H, Nusse R (2012). Wnt/beta-catenin signaling and disease. Cell 149, 1192–1205.

D'Alessandro R, Roselli T, Valente F, Iannaccone M, Capogrosso C, Petti G, Alfano G, Masarone D, Ziello B, Fimiani F, *et al.* (2012). Heart failure: molecular, genetic and epigenetic features of the disease. Minerva Cardioangiol 60, 593–609.

D'Silva NJ, Mitra RS, Zhang Z, Kurnit DM, Babcock CR, Polverini PJ, Carey TE (2003). Rap1, a small GTP-binding protein is upregulated during arrest of proliferation in human keratinocytes. J Cell Physiol 196, 532–540.

Delva E, Tucker DK, Kowalczyk AP (2009). The desmosome. Cold Spring Harb Perspect Biol 1, a002543.

de Rooij J, Zwartkruis FJ, Verheijen MH, Cool RH, Nijman SM, Wittinghofer A, Bos JL (1998). Epac is a Rap1 guanine-nucleotide-exchange factor directly activated by cyclic AMP. Nature 396, 474–477.

Furukawa C, Daigo Y, Ishikawa N, Kato T, Ito T, Tsuchiya E, Sone S, Nakamura Y (2005). Plakophilin 3 oncogene as prognostic marker and therapeutic target for lung cancer. Cancer Res 65, 7102–7110.

Godsel LM, Dubash AD, Bass-Zubek AE, Amargo EV, Klessner JL, Hobbs RP, Chen X, Green KJ (2010). Plakophilin 2 couples actomyosin remodeling to desmosomal plaque assembly via RhoA. Mol Biol Cell 21, 2844–2859.

Godsel LM, Hsieh SN, Amargo EV, Bass AE, Pascoe-McGillicuddy LT, Huen AC, Thorne ME, Gaudry CA, Park JK, Myung K (2005). Desmoplakin assembly dynamics in four dimensions: multiple phases differentially regulated by intermediate filaments and actin. J Cell Biol 171, 1045–1059.

Goossens S, Janssens B, Bonne S, De Rycke R, Braet F, van Hengel J, van Roy F (2007). A unique and specific interaction between alphaT-catenin and plakophilin-2 in the area composita, the mixed-type junctional structure of cardiac intercalated discs. J Cell Sci 120, 2126–2136.

Gosavi P, Kundu ST, Khapare N, Sehgal L, Karkhanis MS, Dalal SN (2011). E-cadherin and plakoglobin recruit plakophilin3 to the cell border to initiate desmosome assembly. Cell Mol Life Sci 68, 1439–1454.
Green KJ, Getsios S, Troyanovsky S, Godsel LM (2010). Intercellular junction assembly, dynamics, and homeostasis. Cold Spring Harb Perspect Biol 2, a000125.
Halbert C, Demers G, Galloway D (1992). The E6 and E7 genes of human papillomavirus type 6 have weak immortalizing activity in human epithelial cells. J Virol 66, 2125–2134.
Hatzfeld M, Haffner C, Schulze K, Vinzens U (2000). The function of plakophilin 1 in desmosome assembly and actin filament organization. J Cell Biol 149, 209–222.
Heid HW, Schmidt A, Zimbelmann R, Schafer S, Winter-Simanowski S, Stumpp S, Keith M, Figge U, Schnolzer M, Franke WW (1994). Cell type-specific desmosomal plaque proteins of the plakoglobin family: plakophilin 1 (band 6 protein). Differentiation 58, 113–131.
Hofmann I, Casella M, Schnolzer M, Schlechter T, Spring H, Franke WW (2006). Identification of the junctional plaque protein plakophilin 3 in cytoplasmic particles containing RNA-binding proteins and the recruitment of plakophilins 1 and 3 to stress granules. Mol Biol Cell 17, 1388–1398.
Hofmann I, Mertens C, Brettel M, Nimmrich V, Schnolzer M, Herrmann H (2000). Interaction of plakophilins with desmoplakin and intermediate filament proteins: an in vitro analysis. J Cell Sci 113, 2471–2483.
Hogan C, Serpente N, Cogram P, Hosking CR, Bialucha CU, Feller SM, Braga VM, Birchmeier W, Fujita Y (2004). Rap1 regulates the formation of E-cadherin-based cell-cell contacts. Mol Cell Biol 24, 6690–6700.
Holthofer B, Windoffer R, Troyanovsky S, Leube RE (2007). Structure and function of desmosomes. Int Rev Cytol 264, 65–163.
Hoshino T, Sakisaka T, Baba T, Yamada T, Kimura T, Takai Y (2005). Regulation of E-cadherin endocytosis by nectin through afadin, Rap1, and p120ctn. J Biol Chem 280, 24095–24103.
Hudson T, Fontao L, Godsel L, Choi H-J, Huen A, Borradori L, Weis W, Green K (2004). In vitro methods for investigating desmoplakin-intermediate filament interactions and their role in adhesive strength. Methods Cell Biol 78, 757–786.
Kirchner F, Schuetz A, Boldt LH, Martens K, Dittmar G, Haverkamp W, Thierfelder L, Heinemann U, Gerull B (2012). Molecular insights into arrhythmogenic right ventricular cardiomyopathy caused by plakophilin-2 missense mutations. Circ Cardiovasc Genet 5, 400–411.
Kitajima Y (2013). New insights into desmosome regulation and pemphigus blistering as a desmosome-remodeling disease. Kaohsiung J Med Sci 29, 1–13.
Koetsier JL, Amargo EV, Todorovic V, Green KJ, Godsel LM (2013). Plakophilin 2 affects cell migration by modulating focal adhesion dynamics and integrin protein expression. J Invest Dermatol 134, 112–122.
Kopperud R, Krakstad C, Selheim F, Doskeland SO (2003). cAMP effector mechanisms. Novel twists for an "old" signaling system. FEBS Lett 546, 121–126.
Kowalczyk AP, Green KJ (2013). Structure, function, and regulation of desmosomes. Progr Mol Biol Transl Sci 116, 95–118.
Kroger C, Loschke F, Schwarz N, Windoffer R, Leube RE, Magin TM (2013). Keratins control intercellular adhesion involving PKC-alpha-mediated desmoplakin phosphorylation. J Cell Biol 201, 681–692.
Lewis JE III, JKW, Sass KM, Jensen PJ, Johnson KR, Wheelock MJ (1997). Cross-talk between adherens junctions and desmosomes depends on plakoglobin. J Cell Biol 136, 919–934.
Li L, Wang S, Jezierski A, Moalim-Nour L, Mohib K, Parks RJ, Retta SF, Wang L (2010). A unique interplay between Rap1 and E-cadherin in the endocytic pathway regulates self-renewal of human embryonic stem cells. Stem Cells 28, 247–257.
McGrath JA, Mellerio JE (2010). Ectodermal dysplasia-skin fragility syndrome. Dermatol Clin 28, 125–129.
McMillan JR, Shimizu H (2001). Desmosomes: structure and function in normal and diseased epidermis. J Dermatol 28, 291–298.
Mertens C, Hofmann I, Wang Z, Teichmann M, Sepehri Chong S, Schnolzer M, Franke WW (2001). Nuclear particles containing RNA polymerase III complexes associated with the junctional plaque protein plakophilin 2. Proc Natl Acad Sci USA 98, 7795–7800.
Mertens C, Kuhn C, Franke WW (1996). Plakophilins 2a and 2b: constitutive proteins of dual location in the karyoplasm and the desmosomal plaque. J Cell Biol 135, 1009–1025.
Moll I, Kurzen H, Langbein L, Franke WW (1997). The distribution of the desmosomal protein, plakophilin 1, in human skin and skin tumors. J Invest Dermatol 108, 139–146.
Moriarty MA, Ryan R, Lalor P, Dockery P, Byrnes L, Grealy M (2012). Loss of plakophilin 2 disrupts heart development in zebrafish. Int J Dev Biol 56, 711–718.
Munoz WA, Kloc M, Cho K, Lee M, Hofmann I, Sater A, Vleminckx K, McCrea PD (2012). Plakophilin-3 is required for late embryonic amphibian development, exhibiting roles in ectodermal and neural tissues. PLoS One 7, e34342.
Nekrasova OE, Amargo EV, Smith WO, Chen J, Kreitzer GE, Green KJ (2011). Desmosomal cadherins utilize distinct kinesins for assembly into desmosomes. J Cell Biol 195, 1185–1203.
O'Keefe EJ, Briggaman RA, Herman B (1987). Calcium-induced assembly of adherens junctions in keratinocytes. J Cell Biol 105, 807–817.
Pasdar M, Nelson WJ (1989). Regulation of desmosome assembly in epithelial cells: kinetics of synthesis, transport, and stabilization of desmoglein I, a major protein of the membrane core domain. J Cell Biol 109, 163–177.
Penn EJ, Burdett ID, Hobson C, Magee AI, Rees DA (1987). Structure and assembly of desmosome junctions: biosynthesis and turnover of the major desmosome components of Madin-Darby canine kidney cells in low calcium medium. J Cell Biol 105, 2327–2334.
Pieperhoff S, Schumacher H, Franke WW (2008). The area composita of adhering junctions connecting heart muscle cells of vertebrates. V. The importance of plakophilin-2 demonstrated by small interference RNA-mediated knockdown in cultured rat cardiomyocytes. Eur J Cell Biol 87, 399–411.
Pieters T, van Roy F, van Hengel J (2012). Functions of p120ctn isoforms in cell-cell adhesion and intracellular signaling. Front Biosci 17, 1669–1694.
Price LS, Hajdo-Milasinovic A, Zhao J, Zwartkruis FJ, Collard JG, Bos JL (2004). Rap1 regulates E-cadherin-mediated cell-cell adhesion. J Biol Chem 279, 35127–35132.
Retta SF, Balzac F, Avolio M (2006). Rap1: a turnabout for the crosstalk between cadherins and integrins. Eur J Cell Biol 85, 283–293.
Rickelt S, Pieperhoff S (2012). Mutations with pathogenic potential in proteins located in or at the composite junctions of the intercalated disk connecting mammalian cardiomyocytes: a reference thesaurus for arrhythmogenic cardiomyopathies and for Naxos and Carvajal diseases. Cell Tissue Res 348, 325–333.
Schmidt A, Langbein L, Pratzel S, Rode M, Rackwitz H-R, Franke WW (1999). Plakophilin 3-a novel cell-type-specific desmosomal plaque protein. Differentiation 64, 291–306.
Schmidt A, Langbein L, Rode M, Pratzel S, Zimbelmann R, Franke WW (1997). Plakophilins 1a and 1b: widespread nuclear proteins recruited in specific epithelial cells as desmosomal plaque components. Cell Tissue Res 290, 481–499.
Shimoyama Y, Hirohashi S, Hirano S, Noguchi M, Shimosato Y, Takeichi M, Abe O (1989). Cadherin cell-adhesion molecules in human epithelial tissues and carcinomas. Cancer Res 49, 2128–2133.
Simpson CL, Kojima S, Cooper-Whitehair V, Getsios S, Green KJ (2010a). Plakoglobin rescues adhesive defects induced by ectodomain truncation of the desmosomal cadherin desmoglein 1: implications for exfoliative toxin-mediated skin blistering. Am J Pathol 177, 2921–2937.
Simpson CL, Kojima S, Getsios S (2010b). RNA interference in keratinocytes and an organotypic model of human epidermis. Methods Mol Biol 585, 127–146.
Sklyarova T, Bonne S, D'Hooge P, Denecker G, Goossens S, De Rycke R, Borgonie G, Bosl M, van Roy F, van Hengel J (2008). Plakophilin-3-deficient mice develop hair coat abnormalities and are prone to cutaneous inflammation. J Invest Dermatol 128, 1375–1385.
Sobolik-Delmaire T, Reddy R, Pashaj A, Roberts BJ, Wahl JK 3rd (2010). Plakophilin-1 localizes to the nucleus and interacts with single-stranded DNA. J Invest Dermatol 130, 2638–2646.
Spindler V, Vielmuth F, Schmidt E, Rubenstein DS, Waschke J (2010). Protective endogenous cyclic adenosine 5′-monophosphate signaling triggered by pemphigus autoantibodies. J Immunol 185, 6831–6838.
Stappenbeck TS, Lamb JA, Corcoran CM, Green KJ (1994). Phosphorylation of the desmoplakin COOH terminus negatively regulates its interaction with keratin intermediate filament networks. J Biol Chem 269, 29351–29354.
Swope D, Li J, Radice GL (2013). Beyond cell adhesion: the role of armadillo proteins in the heart. Cell Signal 25, 93–100.
Takahashi H, Nakatsuji H, Takahashi M, Avirmed S, Fukawa T, Takemura M, Fukumori T, Kanayama H (2012). Up-regulation of plakophilin-2 and down-regulation of plakophilin-3 are correlated with invasiveness in bladder cancer. Urology 79, 240.e1–240.e8.

Tsuruta D, Ishii N, Hashimoto T (2012). Diagnosis and treatment of pemphigus. Immunotherapy 4, 735–745.
Valladares-Ayerbes M, Diaz-Prado S, Reboredo M, Medina V, Iglesias-Diaz P, Lorenzo-Patino MJ, Campelo RG, Haz M, Santamarina I, Anton-Aparicio LM (2008). Bioinformatics approach to mRNA markers discovery for detection of circulating tumor cells in patients with gastrointestinal cancer. Cancer Detect Prev 32, 236–250.
Valladares-Ayerbes M, Diaz-Prado S, Reboredo M, Medina V, Lorenzo-Patino MJ, Iglesias-Diaz P, Haz M, Pertega S, Santamarina I, Blanco M, *et al*. (2010). Evaluation of plakophilin-3 mRNA as a biomarker for detection of circulating tumor cells in gastrointestinal cancer patients. Cancer Epidemiol Biomarkers Prev 19, 1432–1440.
van Triest M, de Rooij J, Bos JL (2001). Measurement of GTP-bound Ras-like GTPases by activation-specific probes. Methods Enzymol 333, 343–348.
Vasioukhin V, Bauer C, Yin M, Fuchs E (2000). Directed actin polymerization is the driving force for epithelial cell-cell adhesion. Cell 100, 209–219.
Wittchen ES, Hartnett ME (2011). The small GTPase Rap1 is a novel regulator of RPE cell barrier function. Invest Ophthalmol Vis Sci 52, 7455–7463.
Wolf A, Krause-Gruszczynska M, Birkenmeier O, Ostareck-Lederer A, Huttelmaier S, Hatzfeld M (2010). Plakophilin 1 stimulates translation by promoting eIF4A1 activity. J Cell Biol 188, 463–471.
Wolf A, Rietscher K, Glass M, Huttelmaier S, Schutkowski M, Ihling C, Sinz A, Wingenfeld A, Mun A, Hatzfeld M (2013). Insulin signaling via Akt2 switches plakophilin 1 function from stabilizing cell adhesion to promoting cell proliferation. J Cell Sci 126, 1832–1844.
Yin T, Getsios S, Caldelari R, Godsel LM, Kowalczyk AP, Muller EJ, Green KJ (2005). Mechanisms of plakoglobin-dependent adhesion: desmosome-specific functions in assembly and regulation by epidermal growth factor receptor. J Biol Chem 280, 40355–40363.